POLITECNICO DI TORINO

Department of Mechanical and Aerospace Engineering

Master's degree in Biomedical Engineering
Master Thesis

3D printing of a cycling helmet with bioinspired structure and biomaterial: design, additive manufacturing, and FEM validation

Supervisors

A. Audenino
I. Torca
J. Aurrekoetxea

Candidate

Giorgia PROSPERI

Torino, October 2021

Euskadirako

Abstract

This thesis work was carried out in collaboration with Mondragon Unibertsitatea, precisely with the research groups of the Departments of Additive Manufacturing and Composite Materials. The objective was to move away from the widespread creation of a Polystyrene (EPS) foam helmet and focus on new material, the Low Weight Polylactic Acid (PLA LW): biodegradable, biocompatible, obtaining a lightweight and 3D printed helmet with a bio-inspired structure (beetle structure), able to absorb a high amount of energy during the impact.

Quasi-static compression tests on EPS samples of a generic helmet and samples of PLA LW with the beetle structure were carried out to establish the differences between the two materials and calculate the specific stress. The PLA LW specific stress values were in an intermediate range between the EPS in the software CES Edupack and the analyzed EPS sample of a generic helmet: a valid reason to continue to carry out tests on the PLA LW with the beetle structure.

The following step was to create the helmet structure with *Grasshopper* (Rhinoceros plug-in) based on the head scan realized with a *3D Sense 2 Scanner* printed the helmet. The printer was a Raise Pro 2 with a double extruder: the first for the PLA LW filament, the second for the water-soluble Polyvinyl Alcohol (PVA). The latter was used for the supports and removed with a dive at the end of printing.

Dynamic tests with *Hoytom HM-D Testing Machine* were performed to analyze the energy absorbed by the EPS and PLA LW with beetle structure helmet models with and without Thermoplastic Polyurethane (TPU) cover. These models were also validated with the Finite Element Method (FEM) in *Abaqus* through explicit dynamic steps.
Finally, further simulations were executed to evaluate the head injury criteria and, in particular, the value of head acceleration, the only parameter considered during a real test and mentioned by the legislation BS EN 1078.

What has been achieved in the physical tests is almost equal absorbed energy of EPS and PLA LW with TPU cover; in FEM analysis these values are slightly higher for PLA LW with bio-inspired structure compared to EPS. The acceleration of the head is lower in the case of the structure bio-inspired with PLA LW, and the objective of not reaching the value of 220g is confirmed.

Contents

List of Tables IV

List of Figures V

1 Introduction 2
- 1.1 Helmet bike protection . . . 2
  - 1.1.1 Helmet structure . . . 3
- 1.2 Additive Manufacturing . . . 4
  - 1.2.1 AM process . . . 4
  - 1.2.2 Materials and techniques - FDM . . . 5
  - 1.2.3 AM in sport . . . 6
- 1.3 3D printed helmets . . . 7
  - 1.3.1 Phases . . . 7
  - 1.3.2 HEXR . . . 8
  - 1.3.3 VORONOI . . . 8

2 State of the art 10
- 2.1 Standards . . . 10
  - 2.1.1 Headform . . . 10
  - 2.1.2 European Standard and American Standard . . . 13
  - 2.1.3 Field of vision - BS EN 1078 . . . 14
  - 2.1.4 Test impact area . . . 15
  - 2.1.5 Anvils and environmental conditions . . . 16
- 2.2 Materials . . . 18
  - 2.2.1 EPS Foam . . . 18
  - 2.2.2 CES Edu Pack - Material selection . . . 19
  - 2.2.3 PLA with natural fiber and PLA LW . . . 21
- 2.3 Bio-inspired structures . . . 24
  - 2.3.1 Beetle structure - Design of the model . . . 25
  - 2.3.2 Specific stress - PLA LW and EPS foam . . . 26

3 Methodology 31
- 3.1 3D scan . . . 31
  - 3.1.1 3D Sense 2 scanner and Meshmixer - Reverse reconstruction . . . 31
  - 3.1.2 3D scan analysis and extraction of features . . . 31

3.2 Helmet design . . . 32
3.2.1 Rhinoceros - Helmet surface . . . 32
3.2.2 Grasshopper - Helmet structure . . . 32
3.3 3D Print . . . 36
3.3.1 Printer and parameters . . . 37

4 Experimental evaluation 40
4.1 Experimental tests . . . 40
4.1.1 Drop-weight impact test machine . . . 40
4.2 PLA LW helmet . . . 40
4.3 EPS helmet . . . 41
4.4 Results . . . 42
4.4.1 First results - PLA-LW and EPS helmet . . . 42
4.4.2 PLA-LW helmet with TPU cover . . . 44

5 FEM Validation 48
5.1 Impactor - Anvils definition . . . 48
5.1.1 PLA LW - Plastic characteristics . . . 49
5.1.2 First test - helmet . . . 51
5.1.3 Second test - plane . . . 52
5.1.4 EPS impact simulations . . . 52
5.1.5 PLA LW impact simulations . . . 54
5.2 Results . . . 55

6 Head Injury Data 57
6.1 Abaqus simulation . . . 57
6.2 Results . . . 60
6.3 Head Injury Criterion . . . 60
6.4 Peak Linear Acceleration . . . 63
6.5 Gadd Severity Index . . . 63
6.6 Diffuse Axonal Injury . . . 65
6.7 Energy absorbed . . . 66

7 Conclusion 67
7.1 Conclusion . . . 67
7.2 Future work lines . . . 68

Bibliography 69

List of Tables

1.1 3D printed helmet steps 7

2.1 Standard specifications 11
2.2 Location of Reference Line [14] 14
2.3 Dimensions about the reference lines in Figure 2.1 and headform masses [6] 14
2.4 Inside circumference of helmet [5] 15
2.5 Table with foam (EPS) density's values 19
2.6 Ashby's method: functions 20
2.7 Ashby's method: objectives 20
2.8 Ashby's method: constrains 21
2.9 Ashby's method: limits 22
2.10 Values about PLA LW tensile tests of MU Additive Manufacturing Department 24
2.11 Compression stress: generic EPS helmet 29
2.12 Compression test: PLA structures 29
2.13 Specific stress calculus, PLA LW and EPS calculus; ρ = density, R = stress, R/ρ [(MPa $*$ m^3)/kg] = specific stress 29

3.1 Printing parameters 38

4.1 Energy absorbed in dynamic test 43

5.1 Mesh element - Kerbstone Anvil 49
5.2 Mesh element - Compression test simulation 50
5.3 Mesh element - plane impact 53

6.1 Mesh element - Head simulation with PLA LW (beetle) helmet 60
6.2 Mesh element - Head simulation with EPS helmet 60
6.3 Head Injury Data - values 63

List of Figures

1.1 The trend of fatalities in crashes involving cyclists and other transport modes [28] 2
1.2 New helmet structure - HEXR design [17] 3
1.3 A summary of additive manufacturing techniques: principle, materials, resolution, and 3D printed sensors in biomedical applications [35] 5
1.4 Example of layer-by-layer print [a], FDM print structure [b] [4] 6
1.5 HEXR design [17] 8
1.6 Voronoi design [3] 9

2.1 Anatomical planes [12] 12
2.2 Principal planes and reference points of a headform [12] 13
2.3 Field of vision (a)(b) [5] 15
2.4 Definition of test impact area [5] 16
2.5 Flat anvil [a] and Kerbstone anvil [b] 17
2.6 (a) The current cycling helmet standard for the EN 1078 [5]; (b) The proposed standard (EN13087-11) as described by the European Committee for Standardization (CEN) [15].[1] 18
2.7 CES EduPack: Mass per unit of compressive stiffness [a], Young's Module and density [b] 23
2.8 SEA of bio-inspired sandwich structures [26] 25
2.9 Beetle structure 26
2.10 EPS generic helmet: helmet pictures [a] [b] and internal structure. External granular structure [c] and pores [d] 27
2.11 PLA LW disks: Grasshopper structure [a], PLA LW structure of 14 mm [b], PLA LW structure compressed [c] 27
2.12 Compression test: Stress-Strain diagrams - EPS 30
2.13 Compression test: Stress-Strain diagrams - PLA LW 30

3.1 Sequence of 3D head scan: 3D scanner acquisition [a], scan after reparation with Meshmixer [b], solid scan: vision frontal and lateral [c] [d] 32
3.2 Feature's extraction: in [a] is represented the impact line, in [b] and [c] two prospective about the definition of the field of vision 33
3.3 SubD representation: lateral view [a], top view [b], front view [c] 33
3.4 Grasshopper diagrams 34

3.5 Construction sequence of the geometry of the helmet 35
3.6 Application of the geometry created to the helmet surface 35
3.7 Grid in the helmet [a], hybrid structure with hexagons and grid [b] [40], compression test results of the hybrid structure [c] [41] 36
3.8 Printing supports 37
3.9 Views of the helmet 39
3.10 Views of the helmet (GH version) 39

4.1 Drop-weight impact test machine [37] 41
4.2 Test 1: PLA-LW helmet 41
4.3 Test 2: PLA-LW helmet 42
4.4 Test 3: EPS helmet 42
4.5 Test 4: EPS helmet 42
4.6 Dynamic machine test - Force 43
4.7 Dynamic machine test - Energy 44
4.8 TPU cover 45
4.9 PLA-LW with TPU - dynamic impact [a] and differences between the helmet with TPU and without TPU cover [b] 45
4.10 Comparison between PLA-LW with TPU and EPS 47

5.1 Kerbstone anvil in the simulation like discrete rigid body [a] and FEM elements [b] 49
5.2 Representation of the samples used for the simulation of the compression test. In Figure [a] the disks of the Hoytom HM-D Testing Machine, in figure [b] the representation of the same as simple surfaces 50
5.3 FEM representation [a] and compression test simulation [b] and real compression [c] 51
5.4 Representation of the two curves related to the simulation in Abaqus of the compression test and the data obtained from the real test to obtain the plastic characteristics of the material 52
5.5 Impact simulation: parts of EPS and PLA helmet 53
5.6 EPS: Boundary conditions and Load 54
5.8 Boundary conditions and Load 54
5.7 EPS impact simulation 55
5.9 PLA impact simulation 56
5.10 EPS and PLA LW energy comparison - Abaqus simulation 56

6.1 My scan head - CAD [a], head imported in Abaqus[b] 58
6.2 Simulation based on BS EN 1078 58
6.3 Simulation based on BS EN 1078 with head 59
6.4 Results simulation based on BS EN 1078 with sectioned head 61
6.5 Head injury risk curves based on HIC values [16] 62
6.6 The abbreviated injury score versus fatality rate [16] 62
6.7 Peak accelerations for both helmets 64

6.8 Peak accelerations for both helmeted and unhelmeted drops. Numbers over bars indicate peak acceleration; For 2 m drop height, results stated are the mean value calculated from three drops [9] 64
6.9 Peak intra-cerebral shearing stress computed with the helmet model coupled to the human head model for all impact points: (a) Flat anvil, (b) Kerbstone anvil [23] 65
6.10 Energy absorption - BS EN 1078 66

Abbreviations

ABS	Acrylonitrile-butadiene-styrene
AM	Additive Manufacturing
ASTM	American Society for Testing and Materials
CAD	Computer Aided Design
CEN	The European Committee for standardization
DAI	Diffuse axonal injuries
EA	energy absorbed
EPS	Expanded polystyrene
FEM	Finite Element Method
FDM	Fused Deposition Modeling
GH	Grasshopper
GSI	Gadd Severity Injury
HIC	Head Injury Criterion
IARV	Injury Assessment Reference Value
NURBS	Non Uniform Rational Basis-Splines
PC	Polycarbonate
PLA	Polylactic Acid
PLA LW	PLA Low Weigh
PLAc	Peak Linear Acceleration
PVA	Polyvinyl Alcohol
RP	Reference point
SEA	Specific energy absorbed
STL	Standard Triangulation Language
SubD	SubDivision surface
TPU	Thermoplastic Polyurethane

Chapter 1

Introduction

1.1 Helmet bike protection

The goal of the thesis was to create a protective device such as a helmet; the choice was to create a bicycle helmet as a result of the analysis of data on trauma and deaths during sports practice and accidents. Falls, bumps can cause brain trauma and during contact and non-contact recreational activities, cycling is among the most at-risk categories of brain trauma, as reported by Coronado et al. [8].

Consulting not only trauma data but also road death data, the sector where there are fatal events is, again, the cycling: is categorized as the most dangerous mode of transport if compared with the percentage of deaths in the event of an accident with motorcycle, car, buses, moped... as shown in Figure 1.1. In addition, the New York Police Department has conducted a study and established percentages on all Bicyclist Fatalities and Serious Injuries in New York City, according to which 74% of general fatal accidents include brain trauma and which, among those by bicycle, 97% includes people without a protective helmet [29]. From these data is derived my choice to devote myself to the field of cycling. Almost all the standards on helmets follow the same fundamental

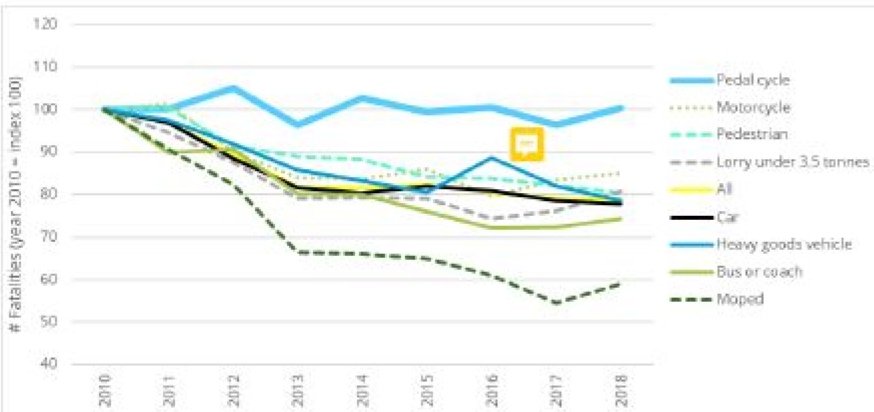

Figure 1.1: The trend of fatalities in crashes involving cyclists and other transport modes [28]

prerogatives, according to which the helmet must remain anchored to the head even after the impact, must resist the penetration of possible objects. It shall be designed to absorb energy during the impact and ensure no brain trauma.

The first helmet with these functions was made by Turner and Havey in the '50s using polymer foam, but their design was hefty and was improved by Roth and Lombard, who modified the helmet's structure, making it more similar to the current one.

1.1.1 Helmet structure

A typical bicycle helmet available on the trade consists of three basic parts, in Figure 1.2:

- **Shell**, is the part visible from the outside of the helmet. Relatively thin, it is able to transfer the energy of the impact to the part below, which has the task of absorbing it to avoid stress concentration at a single point; it absorbs only the initial shock energy; it has a protective function to avoid damage to the internal part which, being foam, can be easily perforated.
  It consists of three categories of materials: *polycarbonate* (PC), *acrylonitrile - butadiene - styrene* (ABS); and *polyolefins* [31]. All have in common a high-impact strength and low production costs.

- **Foam**, is the part that has as the main function to absorb energy during the impact. Generally, it is an *expanded polystyrene* (EPS), lightweight and inexpensive material, whose characteristics will be discussed in Chapter 2.2.1.

- **Straps**, which is the clasp strap, of *nylon* or *polypropylene*.

Figure 1.2: New helmet structure - HEXR design [17]

1.2 Additive Manufacturing

Additive Manufacturing (AM) is a manufacturing process that leads to the 3D printing of a product through 6 main steps. Usually, the two terms AM and 3D Printing are interchanged but do not have the same meaning. If AM indicates the entire production process, the other refers simply to the actual operation. The technique's name suggests a contrast with the classic subtractive production, in which a block of material, the product that it is possible to achieve, is subtracted through the 3D model pre-set. In AM, however, the material is added layer by layer, consistent with the 3D model created.

Among the advantages of using this new technology, it is possible to create objects in a single solution with unique and complex shapes, with a wide range of materials, without worrying about waste production (excluding any media). Especially in applications with metallic powders, this allows cost savings, but also few problems for disposal and pollution, as there is the possibility of recycling the powder that is not used during the production process, making the process green. In addition, production times are considerably lower: the times and costs of realization depend only on the size of the piece and not on its geometric complexity. The problems of AM concern the size of the objects to be created because they depend on the size of the printer you use; just as it is limited, always in correlation with the printer used, the choice of material.

1.2.1 AM process

As previously announced, Additive Manufacturing consists of 6 different steps for the realization:

- **3D model modelling:** it is carried out through Computer Aided Design (CAD) software

- **Generating the .stl file:** for AM, a standard language called Standard Triangulation Language (STL) is used. With this language, the model is modified, and the internal and external surfaces are converted into triangles of different sizes.

- **Model orientation and support generation:** the format .stl is imported into a modelling software (e.g. Simplify 3D). The model will be arranged so that the supports generated to support the object are as few as possible. The supports can be placed to avoid that the body is in contact with the work platform. Avoiding their positioning in areas that need unique surface finishes is necessary, as their removal increases roughness.

- **Slicing:** it is the realization of the different sections that will constitute the model that will be printed. The sections are created using parallel planes that we have parallel at the normal to the z-axis; the planes will be spaced apart by a quantity that depends on the machine's resolution and the parameters imposed.

- **3D Printing:** import of the document into the 3D printer that, layer after layer, will make the object.

- **Subject and treatment:** Once the printing is completed, the object will be obtained with any media. It will require cleaning, removal of supports, and treatments based on the refinement of the surface.

1.2.2 Materials and techniques - FDM

The additive manufacturing techniques currently on the market maybe classified according to the type of source material and can be grouped into three different categories:
1. Additive manufacturing techniques using liquid materials;
2. Additive manufacturing techniques using solid materials;
3. Additive manufacturing techniques using powdered materials.

The following paragraph describes in detail one of the manufacturing techniques an additive called *Fused Deposition Modeling* (FDM), also called melted deposition, this being the technique used to produce the components of the case of study.

3D Printing Methods	Principle	Materials
Fused deposition modelling	Extrusion of constant filament	ABS, PLA, Wax blend, Nylon
Stereolithography	UV initiated polymerisation cross section by cross section	Resin (Acrylate or Epoxy based with proprietary photoinitiator)
Polyjet	Deposition of the droplets of the photo-curable liquid material and cured	Polymer
Selective laser sintering	Laser-induced sintering of powder particles	Metallic powder, polyamide, PVC
3D Inkjet printing	Extrusion of ink and powder liquid binding	Photo-resin or hydrogel
Digital light processing	Photo-curing by a digital projector screen to project layers by squared voxels	Photopolymer and photo-resin

Figure 1.3: A summary of additive manufacturing techniques: principle, materials, resolution, and 3D printed sensors in biomedical applications [35]

FDM printing is one of the most common additive manufacturing technologies; it allows the realisation of thermoplastic polymer objects that are heated and deposited to create an object. The polymer filament is unrolled from the coil using two toothed wheels that push and withdraw the material from the extrusion nozzle; the latter is crossed by the filament and deposits the material to build layer after layer the object. Before the extrusion nozzle, a heating block is positioned to control and adjust the filament temperature above the melting point, escaping the material. An excessively high temperature would cause a casting process that would compromise the machining accuracy; a low temperature would prevent the filament from adhering to the already deposited layer. The extruders move in the XY plane and draw material from two coils (one for the supports and one for the structure), depositing the material for the first layer; Then the platform lowers to allow the realization of the second layer, etc.. is the technique layer-by-layer.

[a] 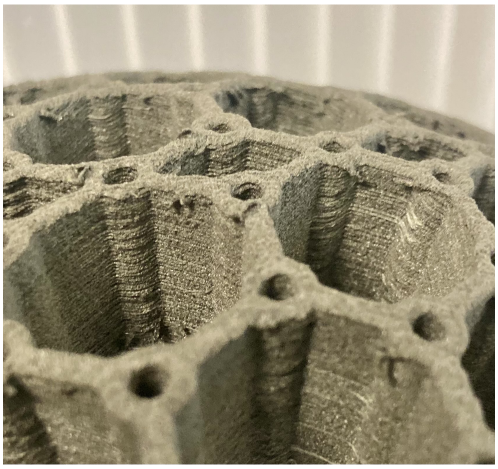

[b] 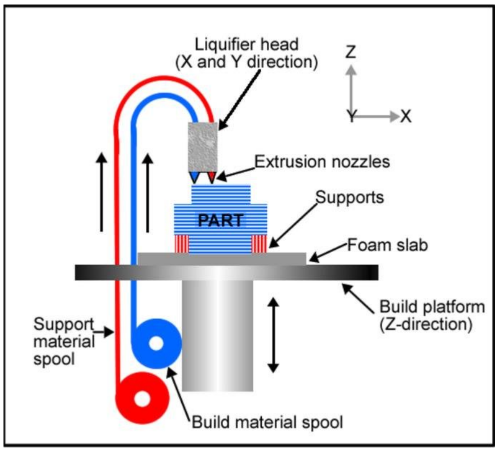

Figure 1.4: Example of layer-by-layer print [a], FDM print structure [b] [4]

Once the processing is completed, it proceeds with the removal of the supports; this activity, usually favoured by the different colours used for the two materials, consists of two phases: initially takes place a coarse removal carried out manually, then the remaining material, in case it is water-soluble as that used for the development of the thesis, is dissolved in water. The work platform instead is characterised by lower temperatures to encourage a rapid hardening of the newly deposited material. Another parameter to be established is the thickness of the layer, which influences the time of realisation of the object and the quality of the finished product. Generally, the printing times of the object vary from a few hours to full days, depending on the size of the workpiece and the resolution chosen.

1.2.3 AM in sport

As described by Novak [27], "sporting products are typically mass-produced to suit normative population physical characteristics such as athlete heights, weights, foot sizes, and limb lengths". The Nike industry began to introduce 3D printing in the sport, producing shin guards, bags, and studs for football shoes. The intuition was that to produce objects with costs and times smaller than the classical production. Currently, the companies that have inserted 3D printing technologies are many, to create unique pieces tailored for sports through reverse engineering with ultralight composites. Meier et. al [21] describe the industries and their respective products; from Nike with spike plate for cleats to Adidas with midsole for running shoe, New Balance with plate and sole for running, Burton with snowboard binding, Redbull and Proto3000 surfboards. The main explanation of these productions lies, as already mentioned, in shorter production times and costs, the reduction of the weight and thickness of the products, the increase of the flexibility thanks to used techniques and materials, the possibility of creating and modifying complex designs.

1.3 3D printed helmets

1.3.1 Phases

Phases about the production of the 3D helmet:

PHASE	CONTENT
1. 3D Scan	- In contrast to the limited number of sizes provided by mainstream helmet brands, the creation of the personal helmet begins with a fitting of the head with a specific app (for Hexr helmet). - The data is then sent to the servers, where a helmet is automatically generated.
2. Structure - Design	Realization of a structure in order to absorb the energy of the impact *Materials:* - Polyamide-11, made from 100% castor bean oil, the most sustainable bicycle helmet (Hexr); - Carbon and fiberglass resin with a polystyrene cover (Voronoi)
3. Industrial 3D printing machines	- Using a technology known as Selective Laser Sintering (SLS): layer upon layer by using high-powered and ultra-fine lasers to melt portions of consecutive layers of powder with a thickness of 0,1mm (Hexr)
4. Assembly	- Assembling: outer shell, chin straps, padding

Table 1.1: 3D printed helmet steps

1.3.2 HEXR

Scientists at University College London developed the HEXR helmet, Figure 1.5, a 3D printed bicycle helmet with a honeycomb structure.
Where? University College London, London.
Designer: Jamie Cook founded HEXR, "after observing energy impacts are different depending upon surface areas. This led him to do extensive research on improving bicycle helmet technology" [17].
How is it made? The first step to realizing the helmet design is to scan the head using a 3D scanner. Once the scan is obtained, thanks to the measurements, the drawing is defined. The honeycomb structure is realized through a print with selective laser sintering technology. The helmet is produced layer upon layer; the process is accurate and employs about 24 hours.
Material: *Polyamide-11*, made from 100% castor bean oil. The use of this material makes the helmet on the market more eco-sustainable: being bio-sustainable and being produced by a production process with little use of water and limited treatments.
App to scan the head: cycling helmet creation process themselves at home (for App-Store) with a fitting cup to scan perfectly the head.

[a] [b]
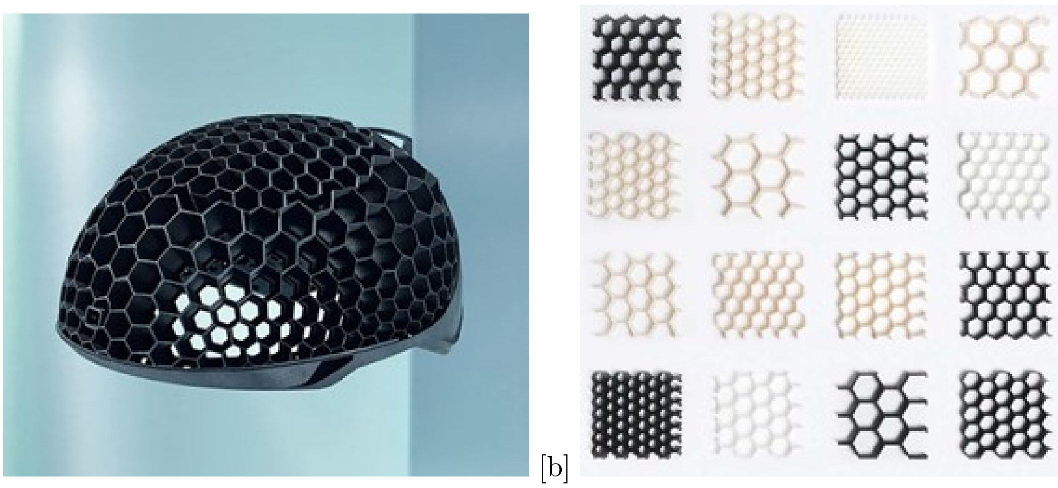

Figure 1.5: HEXR design [17]

1.3.3 VORONOI

The Voronoi, Figure 1.6, the helmet was designed through a program with parametric design, which respected a bio-inspired structure. This inspiration was taken from the conformation of the animal bone and the typical turtle shell.
Where? Nanjing, China
Designer: Yuefeng Zhou, Zhecheng Xu, Haiwei Wang
How is it made? The Voronoi helmet was made through a parameterized design with the use of an unusual mesh. The goal of the structure was to use a minimum amount of material and have a high energy absorption; in this way, it is possible to get a light and

effective product.
Material: The main materials used for the creation of the helmet shell are carbon kevlar and fiberglass resin with a polystyrene lining. The final product is going to be available in 3 sizes and different colours.

Figure 1.6: Voronoi design [3]

Chapter 2

State of the art

2.1 Standards

The specification about the materials, specific tests methods, manufacturing to realize a helmet shall be drawn up by the following standards:

- *American Society for Testing and Materials (ASTM)* is a globally recognized leader in the development and supply of international standards. The World Trade Organization Technical Barriers legislate it to Trade (TBT) Committee.

- *The European Committee for standardization (CEN)* composted by the national body of Austria, Belgium, Bulgaria, Croatia, Cyprus, Czech Republic, Denmark, Estonia, Finland, Former Yugoslav Republic of Macedonia, France, Germany, Greece, Hungary, Iceland, Ireland, Italy, Latvia, Lithuania, Luxembourg, Malta, Netherlands, Norway, Poland, Portugal, Romania, Slovakia, Slovenia, Spain, Sweden, Switzerland, Turkey, and United Kingdom.

In this study the standard specifications show in the Table 2.5 will be taken into account: the first column contains the Standard name, in the designation column the letter with the first number classifies the specification and the second number identifies the year when they were published or the year when the last revision was realized.

2.1.1 Headform

Before realizing a helmet, it is necessary to define the headform. It is the geometrical representation of the head without facial features and ears, but the fundamental axis is represented.

Planes definitions

- *Basic plane*: an anatomical plane that includes the superior rim of the external auditory meatuses (upper edge of the external openings of the ear) and the inferior margin of the orbit (the lowest point of the floor of the eye socket);

STANDARD	DESIGNATION	CONTENT
Standard specification for headforms	F2220-15	This specification identifies the headforms used for testing protective headgear in individual ASTM International test methods and performance standards [12]
Standard specification for helmets used in recreational bicycling or roller skating	F1447-18	This specification recognizes the desirability of lightweight construction and ventilation; however, it is a performance standard and is not intended to restrict design [13]
Standard test methods for equipment and procedures used in evaluating the performance characteristics of protective headgear	F1446-20	These test methods specify equipment and procedures used for testing protective headgear. Individual ASTM performance standards (standard specifications) will use these procedures and equipment. Test conditions, pass-fail criteria, and other performance requirements will be specified in the individual performance standards [14]
Headforms for use in the testing of protective helmets	BS EN 960:2006	This European Standard specifies the dimensional and constructional details of headforms for use in the testing of protective helmets [6]
Helmets for pedal cyclists and for users of skateboards and roller skates	EN 1078:2012+A1	This European Standard specifies requirements and test methods for helmets worn by users of pedal cycles, skateboards and roller skates. Requirements and the corresponding methods of test are given for the following: - construction, including field of vision; - shock absorbing properties; - retention system properties, including chin strap and fastening devices; - marking and information [5]

Table 2.1: Standard specifications

- *Coronal plane*: an anatomical plane perpendicular to both the basic and midsagittal planes and passing through the superior rims of the right and left external auditory meatuses. The transverse plane corresponds to the coronal plane;

- *Midsagittal plane*: an anatomical plane perpendicular to the basic plane and containing the midpoint of the line connecting the notches of the right and left inferior orbital ridges and the midpoint of the line connecting the superior rims of the right and left external auditory meatuses [12]

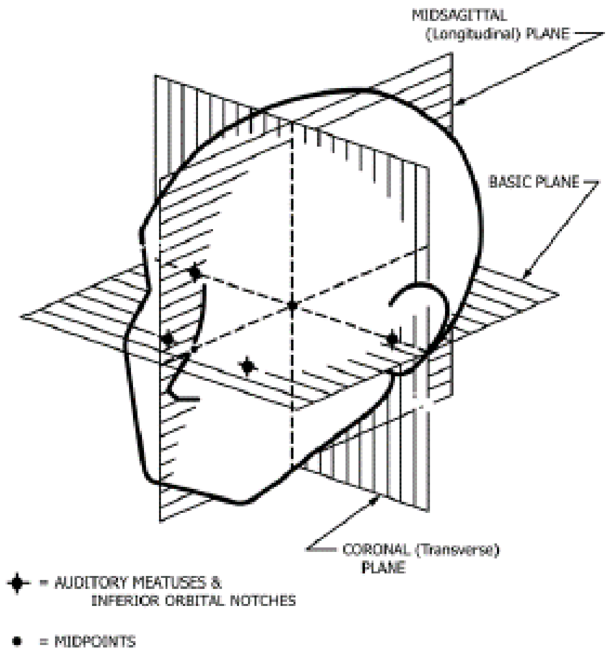

Figure 2.1: Anatomical planes [12]

Planes and reference points

In agreement with the Standard BS EN 960 [6], it is possible to define different characteristic planes, like shown in Figure 2.2:

- *Reference plane*: for a given headform, when erect, the horizontal plane located at a vertical distance 'y' measured down the central vertical axis from the centre of the crown. All horizontal datum levels are quoted relative to this plane;

- *AA" plane*: for a given headform, the horizontal transverse plane is located at a vertical distance 12,7 mm above and parallel to the reference plane. This plane is deemed to correspond to the level of the lower edge of the headband of a helmet. It is the basis upon which the size designation of a helmet may be specified;

- *Central vertical axis*: vertical axis lying along the intersection of the vertical longitudinal plane and the vertical transverse plane;

- *Centre of gravity of the three-quarter headform - point A*: for a given headform, the point on the central vertical axis located at a vertical distance 12,7 mm above the reference plane;

- *Centre of gravity of the full headform - point G*: for a given headform, the point on the central vertical axis located at a vertical distance 'z' below the reference plane;
- *Geometric centre - point R*: for a given headform, the point on the central vertical axis, located at its intersection with the reference plane

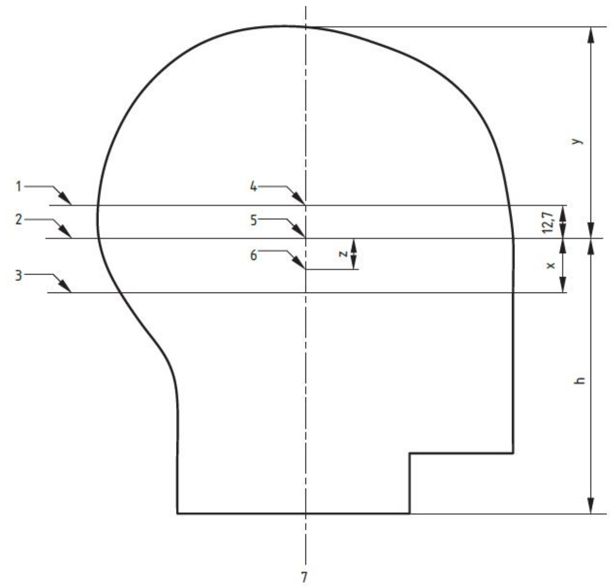

Section on vertical longitudinal plane

Key

1 AA' plane
2 reference plane
3 basic plane
4 point A
5 point R
6 point G
7 central vertical axis

Figure 2.2: Principal planes and reference points of a headform [12]

2.1.2 European Standard and American Standard

Location of gravity centre

Between the European Standard and American Standard, there are differences, the first for the location of the gravity centre:

- *BS EN 960*: the centre of gravity is located within a 10 mm radius of Point G;
- *ASTM F1447*: centre of gravity of the headform must be within a 10° vertical cone from the centre of impact and lie within a rectangular area 28 by 12.8 mm

The size of the head and helmet

- *ASTM F2220*: to measure the external dimension for full headform the distance from the reference plane to the top of the headform. There are different dimensions F2220 (A, if the measure is 89,7 mm – C with 93 mm – E with 96 mm – J with 102,5 mm – M with 107 mm). Then, with this classification, it is possible to extract the dimension of x,y,z (mm) with the following Table 2.2:

Headform Label	X, mm	Y, mm	Z, mm
F2220-A	24.0	89.7	11.1
F2220-C	25.0	91.2	11.5
F2220-E	26.0	96.0	11.9
F2220-J	27.5	102.5	12.7
F2220-M	29.0	107.0	13.3
F2220-O	30.0	110.0	13.7

Table 2.2: Location of Reference Line [14]

- *BS EN 960*: to obtain the size designation and the headform masses this Standard considers the measure of x,y,z (mm) in Figure 2.1. The possible designation are 21: from 445 to 645, some of these are shown in the Table 2.3:

Thanks to the size designation with the Standard BS EN 1078 there is the possibility to define the inside circumference of the helmet, and this it is shown in the following Table 2.4.

Size designation	h (mm)	x (mm)	y (mm)	z (mm)	Mass (g)
445	108,5	21,0	81,7	9,9	
595	140,0	28,5	105,4	13,1	
605	142,1	29,0	107,2	13,3	5 600 ± 160

Table 2.3: Dimensions about the reference lines in Figure 2.1 and headform masses [6]

2.1.3 Field of vision - BS EN 1078

Apply a load of 50 N on the crown of the helmet in order to stabilize the helmet on the headform. To avoid having an occultation of the visual field, Figure 2.3, it is better to follow this angle measures [5]:

- **horizontally**: min. 105 ° from the longitudinal vertical median plane to the left and right hand sides
- **upwards**: min. 25 ° from the reference plane
- **downwards**: min. 45 ° from the basic plane

Size designation (EN 960:1994 equivalent)	Inside circumference of helmet mm
495 (A)	500
515 (C)	520
535 (E)	540
555 (G)	560
575 (J)	570
585 (K)	580
605 (M)	600
625 (O)	620

Table 2.4: Inside circumference of helmet [5]

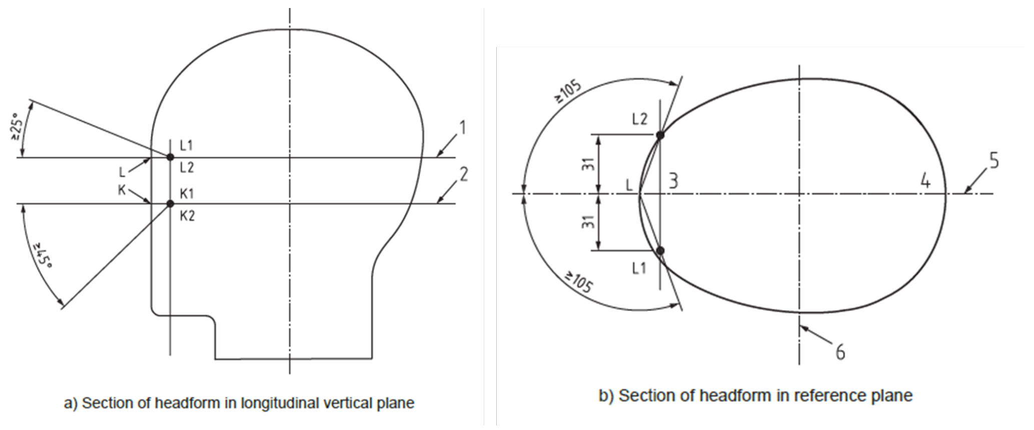

Figure 2.3: Field of vision (a)(b) [5]

2.1.4 Test impact area

Standard EN 1078 will be considered for this study, which defines the parameters helpful in performing the shock absorption test. The drop test impact consists of an impact on two anvils of flat surface or kerbstone.

In the Standard is specified the Test Area where the impact is to be performed. The first thing is to apply a vertical load of 50 N on the crown of the helmet in order to

stabilize the helmet on the headform [5].
1. Draw the AA" line (in the AA' plane) on the helmet
2. Draw a line on the helmet, parallel to and approximately 20 mm above the AA" line (for use as an angular measurement datum line)
3. Mark the helmet at points B1 and B2. These points are the sideways horizontal projection of point B onto the outer surface of the helmet
4. Draw a line RR' on the helmet passing through B1 and B2, the line being angled 10° upwards toward the front of the helmet relative to the datum line drawn in d). The area above the line drawn in f) is the test area for impacts on the flat anvil. The area above the line RWA" is the test area for impacts on to the kerbstone anvil.

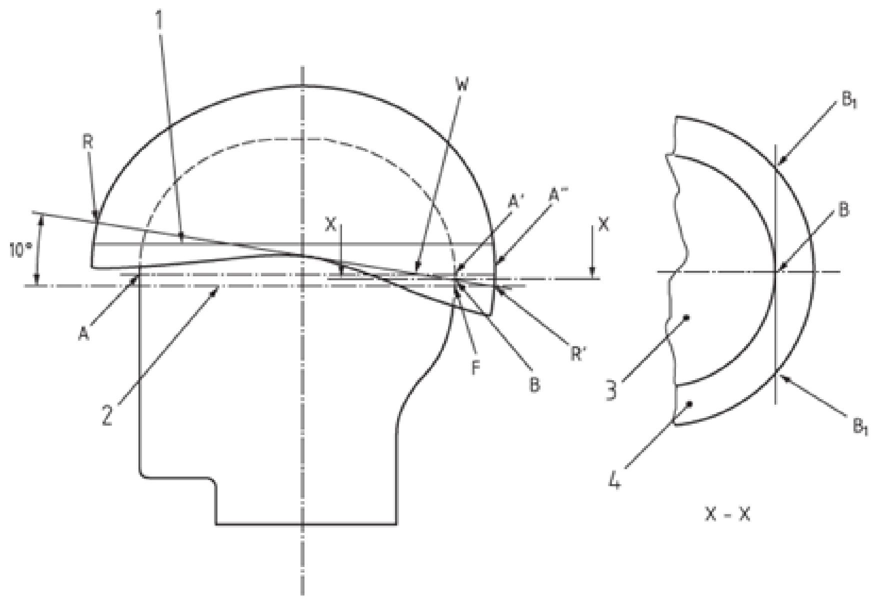

Figure 2.4: Definition of test impact area [5]

2.1.5 Anvils and environmental conditions

EN 1078

During the validation process, each of the 30 helmet target points was impacted experimentally and numerically under three environmental conditions (-20°C, +50°C, and humidity).

The impact should never exceed 250 g for impacts with velocities corresponding to 5,42 m/s on a flat anvil and 4,57 m/s on a kerbstone anvil. These are theoretically equivalent to 1497 mm and 1064 mm drop heights, respectively [5]. About the characteristics of the anvils, according to EN 1078, these depend on the type, in the case of:

- **Flat anvil**: it has a circular form with a diameter of 130 ± 3 mm with 25 mm of thick

- **Kerbstone anvil**: face inclined at 52.5 ± 2.5° to the vertical and edge with a radius of 15 ± 0.5mm. The height shall be not less than 50 mm, and the length not less than 125 mm [5]

According with the regalement EN 1078 [5] it has been possible to realize the volumes: in this work, the Flat anvil has a diameter of 130 mm and a height of 25 mm, the kerbstone anvil has a horizontal edge of 130 mm, a height of 51 mm, a length of 126 mm and the edge that impacts the helmet has a radius of 15 mm. The anvils are represented in Figure 2.5.

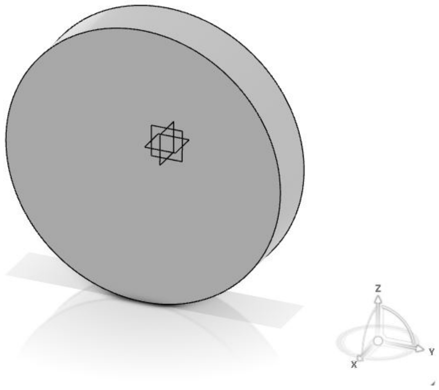

[a]

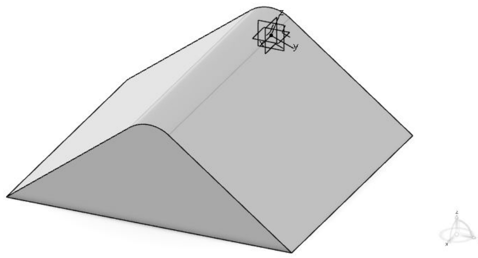

[b]

Figure 2.5: Flat anvil [a] and Kerbstone anvil [b]

EN 13087-11 (Proposal)

A proposal of November 2018 (EN 13087-11) talks about oblique impact tests (Rotational test method) [15]. Define a method to measure rotational energy absorption in tangential impacts in short duration impact situations; the velocity considered by Adanty et al. [1] is 6.5 m/s. The same anvils of the Standard EN 1078 are used, the flat anvil and the Kerbstone anvil, but the difference is the vertical drop towards an impact angle, between 30-60°; the degree considered by Adanty et al. [1] is 45°.

Three different rotations are considered [34]:

- **Rotation around X-axis**: contact point on the side of the helmet resulting in a rotation around X-axis. Initial position of the headform X-, Y- and Z-axis 0°
- **Rotation around Y-axis**: Contact point on the upper part of the helmet resulting in a rotation around Y-axis. Initial position of the headform X-, Y- and Z-axis 0°
- **Rotation around Z-axis**: Contact point on the upper part of the helmet resulting in a rotation around Y-axis. Initial position of the headform X- and Z-axis 0° and 65° around Y-axis

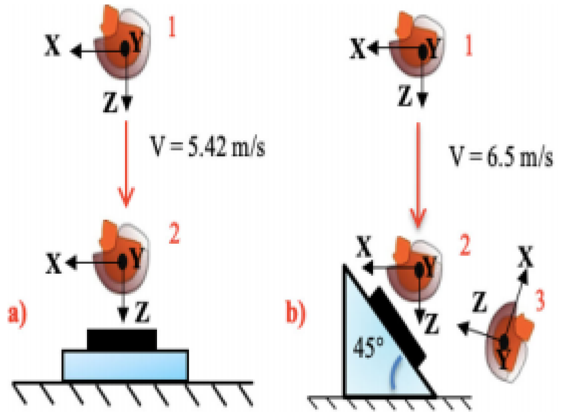

Figure 2.6: (a) The current cycling helmet standard for the EN 1078 [5]; (b) The proposed standard (EN13087-11) as described by the European Committee for Standardization (CEN) [15].[1]

2.2 Materials

2.2.1 EPS Foam

As mentioned in Chapter 1.3, the material most commonly used for making the helmet is the EPS. Mustafa et al. [25] analysed the EPS with four different density values of 50 kg/m^3, 64 kg/m^3, 80 kg/m^3 and 100 kg/m^3. "The drop impact simulation model was used to test the impact attenuation of the helmet with different densities. The drop test was performed on four impact locations: top, front, and sides".

The impact velocity of the helmet and headform was set at 5.44 m/s. The lowest peak linear acceleration was recorded at the top location and a density of 64 kg/m^3, with 148.14 g. This study sets out to determine the effect of the user-centered helmet design with different foam densities (from 50 kg/m^3 to 100 kg/m^3) on the impact attenuation of the bicycle helmet.

Kroeker et al. [19] tested the helmets at three impact speeds: 3.0 $\pm$ 0.01 m/s, 6.3 $\pm$ 0.02 m/s, and 7.8 $\pm$ 0.01 m/s.

They established the mean value about bulk density in a helmet with EPS foam is 66,6, considering HIC and Peak Acceleration test. The global range is between 64 kg/m^3 and 75 kg/m^3.

Kroeker et al. [20] established the foam for kids helmets is 64-88 kg/m^3, and for the traditional helmets is 60-100 kg/m^3.

Trzaskalska et al. [36] controlled the influence of polymer liner density on energy absorption during impact. They discovered the best properties have samples whose density is between 54 to 60 kg/m^3.

Cui et al. [10] considered the density of each layer from the values of 25, 50, 60, 80, and 100 kg/m^3 and they realize a 45 grades side impact and normal crown impact. The result is a density of 64 kg/m^3.

Wei et al. [38] discovered from their test results that EPS has a buffer layer density of 60 kg/m^3 is the most reasonable.

Foam density's values - Literature	
Authors	**Density's values**
Mustafa et al. [25]	64
Kroeker et al. [19]	64 - 75
Kroeker et al. [20]	60-100 (traditional) and 64-88 (kids)
Trzaskalska et al. [36]	54 - 60
Cui et al. [10]	54
Wei et al. [38]	60

Table 2.5: Table with foam (EPS) density's values

The other are mean values obtained by CES EduPack's program about this material:

- Density $\rho = 64.51$kg/m^3
- Young's Module E = 27,5 MPa
- Poisson's ratio ν = 0,275
- Yield's stress σ= 0,9 MPa
- Elongation at fracture = 4,5%

2.2.2 CES Edu Pack - Material selection

CES Edupack software was used to satisfy the idea of creating a lightweight helmet by printing it in 3D and having the possibility to insert the desired characteristics of the material and, therefore, select it. To make a choice, I used level 3 of engineering (advanced), selecting the following criteria of the material: bio-material, biodegradable, a polymer of concentration 20 - 100 %, which complies with the 'European Restriction on Hazardous Substances (Rohs) standards' regarding the composition of the material, ensuring that it does not contain a high percentage of toxic substances compared to the established percentage. In addition, it must have proper durability in contact with cold water (imagining a possible rain) and 'good' durability to UV radiation.

According to Ashby's method, [2], to select a material, it is possible to follow the following steps:

1. Establish the *function* of the product: What does the component do? The helmet is an instrumental use to protect the head during an impact; this characteristic depends on materials and qualities. It can prevent an injury, which depends on materials and design because it has to be of the right head size. It would be comfortable because it must be worn, and it must give security to the person wearing it (by design). In the following Table 2.6 the analysis of the functions:

Ranking	Function description	Depends on
1	Head protection (energy absorbing)	Material
2	Head protection (energy absorbing)	Design
3	Head protection (injury prevention)	Material
4	Head protection (injury prevention)	Design
5	Comfortable	Material
6	Comfortable	Process

Table 2.6: Ashby's method: functions

2. The *objectives* that are targets for the design: the material is to be maximised or minimised?
To manufacture and market a product, objectives such as minimizing weight, cost or environmental impact must be considered. In the following Table 2.7 the analysis of the objectives:

Ranking	Title	Objectives description
1	Mass	Minimize: The mass has to be the same or lower
2	Cost	Minimize: everyone should have the opportunity to buy it
3	CO2 footprint	Minimize CO2 emission
4	Corrosion	Minimize: high strength, because it can be in contact with the water
5	Pleasant to touch	Maximize: it is not a rough material because it has to put on and put off by hands
6	Refractive index	Minimize: it must not reflect light

Table 2.7: Ashby's method: objectives

3. Definition of *constrains*: What essential conditions must be meet?
Establish constraints is essential to complete the function of the instrument. Examples of constrains are, Table 2.8:

4. The *limits:* characteristic independent of the material that does not influence the physical properties. In the following Table 2.9 the analysis of the limits:

Title	**Loading case**	**Constraints description**	**Material index (Max-Min)**
Stiffness	Column in compression / Tie in tension	Mass	Min
Stiffness	Column in compression / Tie in tension	Cost	Min
Stiffness	Column in compression / Tie in tension	CO2	Min
Strength	Column in compression / Tie in tension	Mass	Min
Strength	Column in compression / Tie in tension	Cost	Min
Strength	Column in compression / Tie in tension	CO2	Min

Table 2.8: Ashby's method: constrains

2.2.3 PLA with natural fiber and PLA LW

Initially, the best material that met the desired criteria was searched. From this study, it was found that the material closest to having the required characteristics is the PLA 30% natural fiber, as shown in the Figure 2.7, which shows the graphs obtained relating to the relationships between Young's Module and density, the objective to reduce the mass per unit of compressive stiffness and strength, to reduce the CO2 footprint per unit of stiffness and strength and mass per unit of compressive strength.

Performance index IR

The stiffness criterion has the following characteristics:

$$m = A * L * \rho \tag{2.1}$$

$$\epsilon = \frac{\sigma}{E} = \frac{\frac{F}{A}}{E} \tag{2.2}$$

$$A = \frac{F}{\epsilon * E} \tag{2.3}$$

Ranking	Title	Function description
1	Biocompatibility	It is the ability of a material the ability of the material not to cause any local or systemic adverse response in the recipient of the material
2	Biodegrability	Biodegradable material do not biodegradable under anaerobic conditions
3	Biomaterials - all	The terms is used for biological, natural, bio-derived, bio-inspired material
4	RoHS (EU) Compliant grades	Restriction of the use of certin prohibites substances (mercury, cadmium hexavalent chromium...)
5	Polymer	20-100% (from the table with Plastic polymers)
6	UV	Resistance at UV sunlight

Table 2.9: Ashby's method: limits

$$A = \frac{F * L * \rho}{\epsilon * E} \tag{2.4}$$

With fixed variables:
- F (the load), L (the length),
With variables that depend on the material:
- E (Young's Module), ρ (density)

In general, when a chart is created, the distribution of the mass is represented in the following modality like in Figure 2.7 [b], where the materials above the line have a lower mass, while those below a greater mass.

Following the results of the CES Edupack program that had selected the PLA with natural fibers as the best, the first print of the helmet was made with this material, using as support the PVA. Initially, the result seemed satisfactory, the helmet had a high definition, but a fundamental problem was found by reducing the helmet in the water to allow the supports of PVA to dissolve. In the act of diving, in fact, after ten minutes some parts of the helmet, especially the front and rear, have disintegrated, making the helmet unusable. Because of this problem, it was necessary to change the material.

[a]
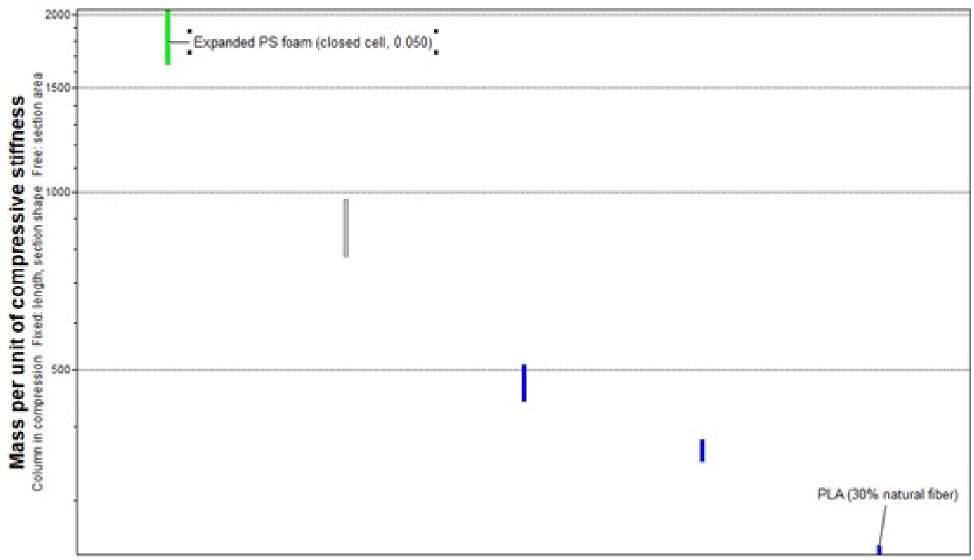

[b]
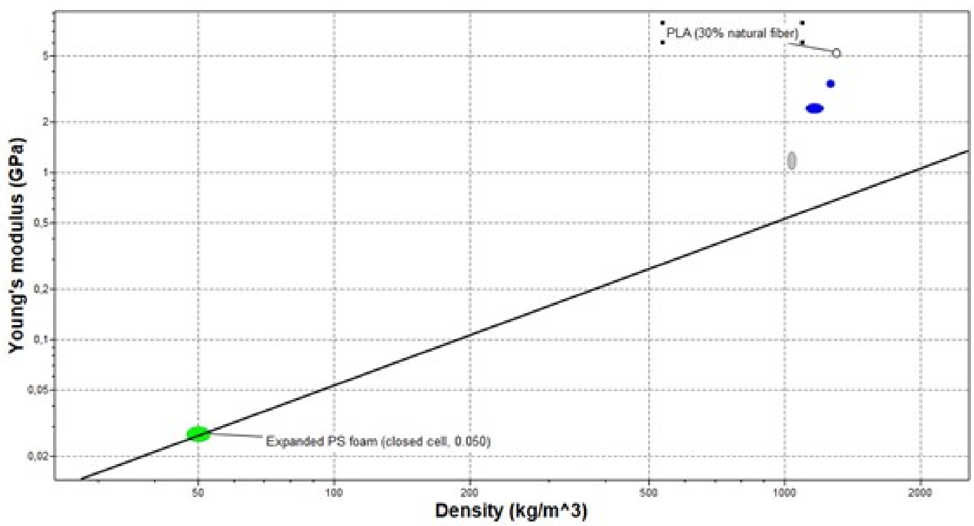

Figure 2.7: CES EduPack: Mass per unit of compressive stiffness [a], Young's Module and density [b]

Further investigations carried out by the Mondragon Unibertsitatea Additive Manufacturing Department revealed a new material, the PLA Low Weight, which, during 3D printing, allows to obtain a weight of 65 % lower than that which could be obtained from the classic PLA, as reported in the technical sheet of the filament produced by the company Colorfabb [7].

The investigation team of the Composite Department carried out tensile tests with samples 3D printed at different temperatures as suggested by the manufacturer to obtain the technical characteristics. The temperatures examined are: 200°, 220°, 250°, 260°. The datasheet shows the density can have values between 0,4 - 1,24 g/cm^3; the bed has to have a temperature between 50 - 60°, the printing speed has to have values between 40 - 80 mm/s. This typology of PLA is expandible, so much that "At around 230 ° this material will start foaming, increasing its volume by nearly three times." [7].

T[°C]	Section [mm^2]	Volumen [mm^3]	Mass [g]	ρ[kg/m^3]	E [N/mm^2]
200	42,235	1030,117	1,2	1165	3288,07
220	43,805	1655,821	1,8	1087	2657,95
250	52,412	1948,139	1,7	873	1780,58
260	59,655	1454,377	1,2	825	1170,47

Table 2.10: Values about PLA LW tensile tests of MU Additive Manufacturing Department

From the tests that have been carried out on the material at different temperatures, the printed sample is better at 250° with a volume of 1948,139 mm^3 and a section of 52,412 mm^2, as shown in Table 2.10. For this reason the specific of the material that have been taken into consideration are the following:

- Density ρ = 873 kg/m^3
- Young's Module E = 1750 MPa
- Poisson's ratio ν = 0,33
- Yield's stress σ = 29,48 MPa
- Elongation at fracture = 4,91%

2.3 Bio-inspired structures

When we talk about bio-inspired structures to nature, we refer to structures that allow obtaining a low weight for the model that is realized and excellent absorption energy during the impact. Recently the structures that have been most used in the biomimetic field are the "columns structures, sandwich structures, plates, honeycomb, and foams"[26], but aiming to achieve a structure increasingly with high absorption energy, new structures, derived from plants and animals, such as beetle, horsetail, turtle, bird beak, have been analyzed. The first to create multi-cells tubes, helicoidal structures, the second to multi-corner tubes. [26].

The authors analyze the specific energy absorbed (SEA) by bio-inspired sandwich structures per unit mass, which can be derived from the following equation:

$$EA(d) = \int_0^{d_{max}} F(x)dx \tag{2.5}$$

$$SEA(d) = \frac{EA(d)}{m} \tag{2.6}$$

Where EA is the energy absorption, "mainly used to evaluate an energy absorber's ability to dissipate crushing energy through plastic deformation", F(x) is the crashing force, d_{max} is the effective deformation distance [26].

What derived from their investigations is that having regard to a density of between 0 and 1000 kg/m^3, the volumetric energy absorbed is higher for the beetle-inspired structures than the others, as shown in Figure 2.8. Based on this consideration it was chosen to draw the helmet following this geometry.

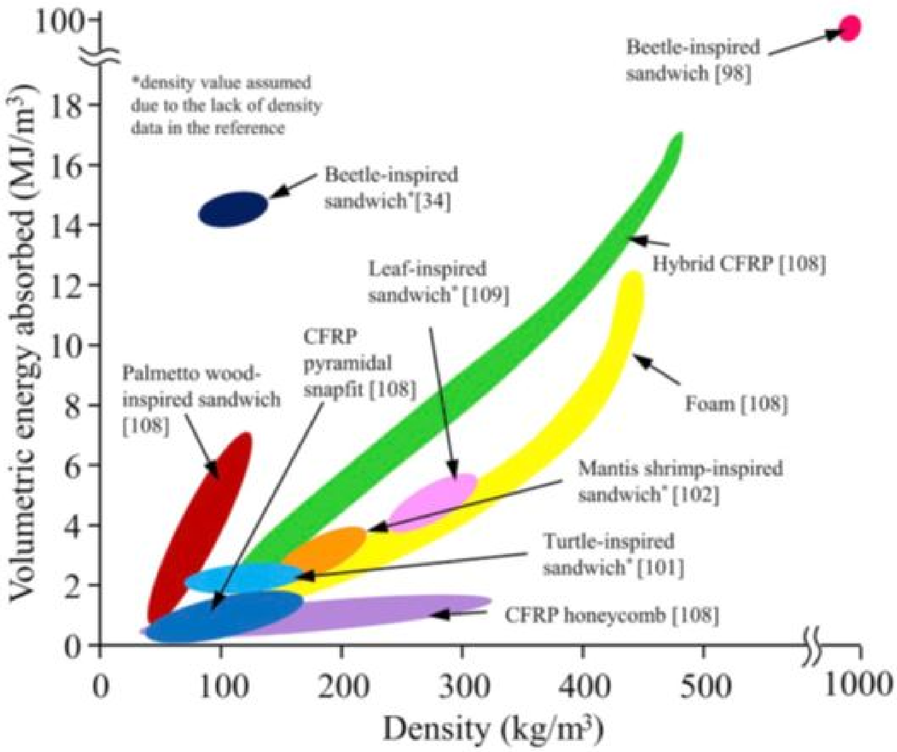

Figure 2.8: SEA of bio-inspired sandwich structures [26]

2.3.1 Beetle structure - Design of the model

To develop and increase lightweight, high-strength, and optimize bio-mimetic functional and structural materials, the trabecular structure of the beetle elytron is studied. The single structure is realized following the requirements cited by Zhang et al. [39].

To realize the beetle's structure, it is not enough to have information about the length of the side of the hexagon and the thickness, but it is also necessary to take into account the relationship between the diameter of the circumferences present on the vertices of the hexagon and the measurement of the side. The representation of a single cell is in Figure 2.9. It is shown in [a] a general structure with an edge of 12 mm, circumference's diameter of 6 mm, and thickness of 1,6 mm; in [b] is shown the height of 20 mm.

For the construction of the helmet a thickness of 1,2 and 1,6 mm was used; the image concerns a proportion between the length of the hexagon side and the diameter of the circumference. The side (distance between the centers of two circumferences) is twice the diameter measurement.

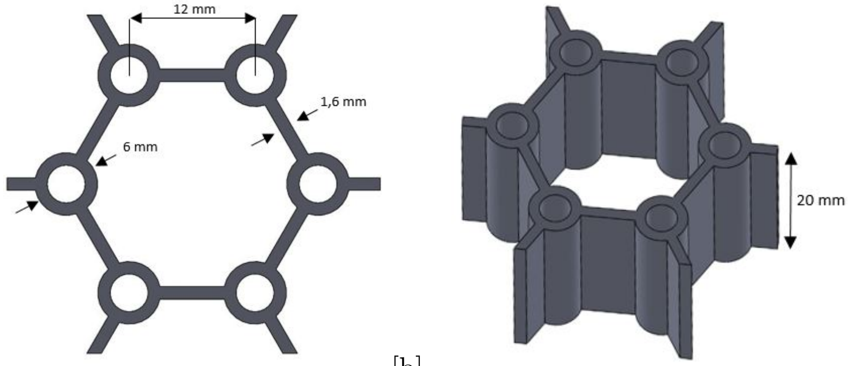

[a] [b]

Figure 2.9: Beetle structure

2.3.2 Specific stress - PLA LW and EPS foam

To test the beetle structures, compression tests were investigated. The PLA LW structure was inserted in a 'disk', with a diameter of 100 mm and a height of 20 mm. The area and the volume of the disk is, correspondingly, 7854 mm^2 and 1,57 * 10 mm^3. The structures examined have different dimensions: the edge L (distance between two centers of the circumferences) had the following measures: 9, 10, 12, 14, 16 mm, the thickness of the circumferences and edges are respectively of 1,6 mm for every structure and 1,2 mm for the structure with L = 16 mm.

The test was carried out with the Hoytom HM-D Testing Machine; with capacities between 5 and 100 kN. The test models were subjected to displacement loading at a rate of 1 mm/min, as referenced by Chen et al.[18] with a cylindrical specimen. The specific stress of the structures was compared with the specific stress of a generic EPS helmet; the photos about it are shown in Figure 2.10. The EPS helmet structure is granular with pores inside. The different grains dimension and these pores can be the reason for which the Stress's values are between two values 0,7 and 1,16 MPa.

Four parts of the EPS helmet were considered in the test; the dimension and relative characteristic are in the Table 2.11, where m = mass, A = area, F = load, ρ = density, R = stress, R/ρ = specific stress. To calculate the values of stress about PLA structures and EPS foam, compression test graphs were been analyzed. The stress value for each structure was calculated considering the single load, the single area, and the average density value (140,55 [kg/m^3]).

The stress values of the PLA structures (Figure 2.11) and other characteristic values are in Table 2.12, where m = mass, A = area, F = load, ρ = density.

Figure 2.10: EPS generic helmet: helmet pictures [a] [b] and internal structure. External granular structure [c] and pores [d]

Figure 2.11: PLA LW disks: Grasshopper structure [a], PLA LW structure of 14 mm [b], PLA LW structure compressed [c]

The results of the load-displacement graphs are affected by the geometry of the disk; the target is to valid for any shape or size; for this is preferred to realize a diagram that depends from σ (or stress) and the deformation ϵ (or strain) which can be defined respectively as:

$$\sigma = \frac{F}{A_0} \tag{2.7}$$

$$\epsilon = \frac{l - l_0}{l} \tag{2.8}$$

where F is the load during the test, A_0 is the area, l_0 is the initial length and l is the length when the load is applied. The areas considered for the EPS cube is reported in Table 2.11 in the second column; the areas of the PLA structure is 7854 mm^2, like the area of the circumscribed disk.

The values compared are shown in Table 2.13, and the graphs obtained by Matlab code to analyze the recorded data of the compression machine are in Figure 2.13 and in Figure 2.12.

Considering that the data provided by the compression machine are subject to noise and disturbances, it was decided to convert the original curve into polynomial type curves that allow obtaining the best interpolating curve for the data in question. To obtain them it was divided the recorded data into two groups: the first part from 0 until the end of the linear part and the second when the curve becomes linear again. The best-fitting (in the least-squares sense) was performed using the *polyfit* and *polyval* functions of Matlab. The first returns the coefficients of the p(x) with n degree, the second evaluates p(x) at each point in x. The polynomial formula p(x) is shown in the Equation 2.9.

$$p_n(x) = a_n x^n + a_{n-1} x^{n-1} + ... + a_2 x^2 + a_1 x + a_0 \tag{2.9}$$

where $a_0, ..., a_n$ are constants and x is the indeterminate. The choice of the degree of the polynomial was made based on the criterion of wanting to obtain linear curves that respected the elastic trend at the beginning of the graph. For this reason, the degree of the polynomial is 1. Subsequently I searched through the intersection of the two lines for the point that is equivalent to the maximum stress that marks the end of linearity.

This value for EPS and PLA LW is the R [MPa] in the Table 2.13. The average stress value for PLA LW is 1,39 MPa and for EPS is 0,94 MPa. The specific stress (R/ρ) is 18 MPa $*$ m^3)/kg for the EPS found in CES, 6,69 MPa $*$ m^3)/kg for the EPS foam of the generic helmet, and for PLA LW is 11,61 MPa $*$ m^3)/kg, an intermediate value between the two, which is what we wanted to achieve.

m [*g*]	**A** [$\mathbf{mm}^2$]	**F** [N]	ρ [$\mathbf{kg/m}^3$]
EPS (CES)			50
1,6	923,4	1063	138,64
1,8	879	593	136,51
2,1	858	833	142,37
2,4	864	564	144,68
Average value			140,55

Table 2.11: Compression stress: generic EPS helmet

L [mm]	**t** [mm]	**m** [g]	**F** [N]	ρ [$\mathbf{kg/m}^3$]
9	1,6	21,4	7250	136,3
10	1,6	19,2	5560	124,67
12	1,6	20,1	8190	130,51
14	1,2	13,8	8000	89,61
Average value				120,27

Table 2.12: Compression test: PLA structures

PLA LW structure ρ= 120,27kg/m^3			EPS structure ρ= 140,55kg/m^3		
Edge [mm]	**R** [MPa]	**R**/ρ*10^3	Number	**R** [MPa]	**R**/ρ*10^3
			EPS (CES)	0,9	18
9	1,73	12,69	1	1,16	8,24
10	1,39	11,14	2	0,8	5,68
12	1,38	10,57	3	1,05	7,46
14	1,08	12,05	4	0,77	5,40
Average value	1,39	11,61		0,94	6,69

Table 2.13: Specific stress calculus, PLA LW and EPS calculus; ρ = density, R = stress, R/ρ [(MPa $*$ m^3)/kg] = specific stress

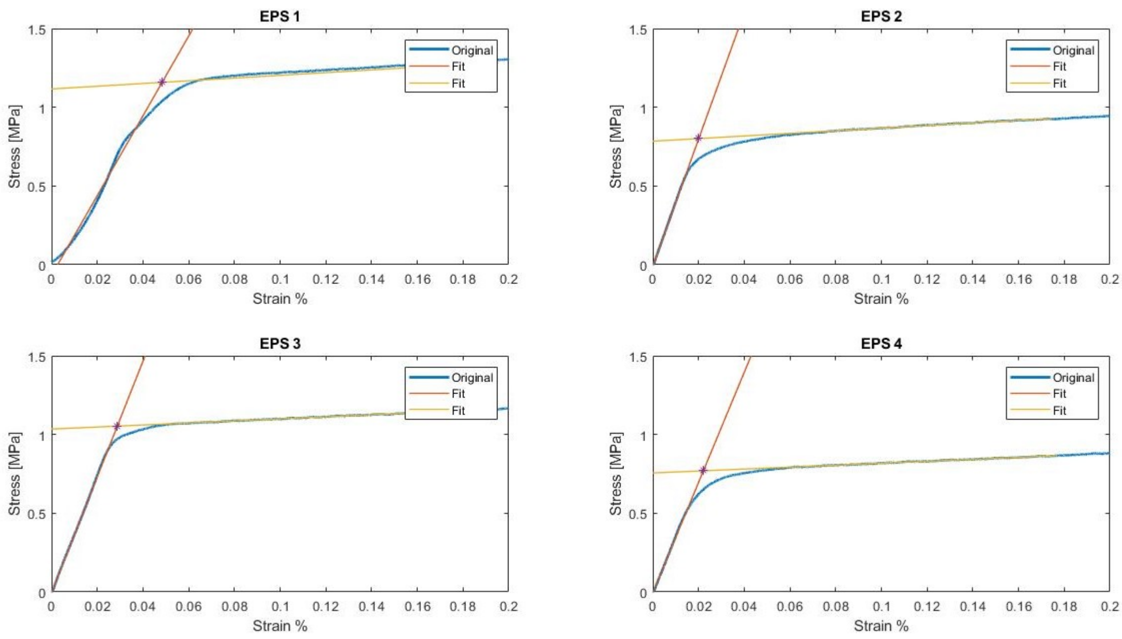

Figure 2.12: Compression test: Stress-Strain diagrams - EPS

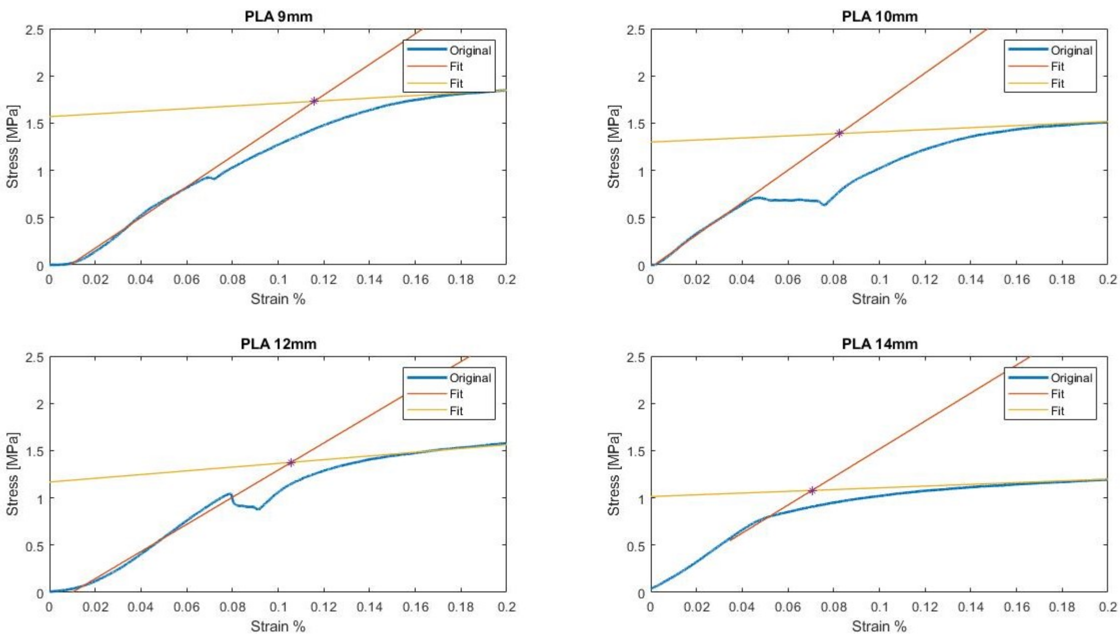

Figure 2.13: Compression test: Stress-Strain diagrams - PLA LW

Chapter 3

Methodology

3.1 3D scan

3.1.1 3D Sense 2 scanner and Meshmixer - Reverse reconstruction

Standardized measures were not taken into account for making the helmet, but the size was obtained through a 3D scan of my head.

The scanner used is *3D Sense 2* by 3D Systems, which has a minimum scanning volume of 20 x 20 x 20 cm and a maximum scanning volume of 300 x 300 x 300 cm. To scan my person, I was helped to get a full view at 360 ° at an appropriate distance. Real-time visualization of the captured images was shown through 3D Sense software. The idea of scanning the head with the scanner refers to the methodology used by Wang et al. [30]. They used a reverse reconstruction, functional for me to realize the helmet surface made to measure my head, and, like them, a silicone pool cap was used to make scanning as smooth as possible. The authors claim the head scan "can also be used to obtain information about the object's surface, which is then reconstructed utilizing the computer's three-dimensional model via reverse modelling software" [30] that, in my case, is *Autodesk Meshmixer*.

The files it was could get from the scan were .stl, .obj, and .ply format; they were exported to .obj to work, in the next step, with *Autodesk Meshmixer* that allowed to modify and homogenize the 3D image obtained from the scan.

In Meshmixer, through the selection and delete commands, the superfluous parts were deleted that had been acquired and, with the inspector and the Draw/Draw2 commands the vertices were moved locally along a pre-defined direction and with Smooth the surface more homogeneous was made. The sequence of steps is shown in the Figure 3.1.

3.1.2 3D scan analysis and extraction of features

In Chapter 2 the directives imposed by the BS EN 960 Standard were examined, concerning the definition of the helmet and the measures to be respected in the field of vision, and the part of the helmet was to carry out impact tests.

In Figure 3.2, the features defined complying with the Standard's rules are represented. To define these features, the software *NX* was used. The angle in the subfigure

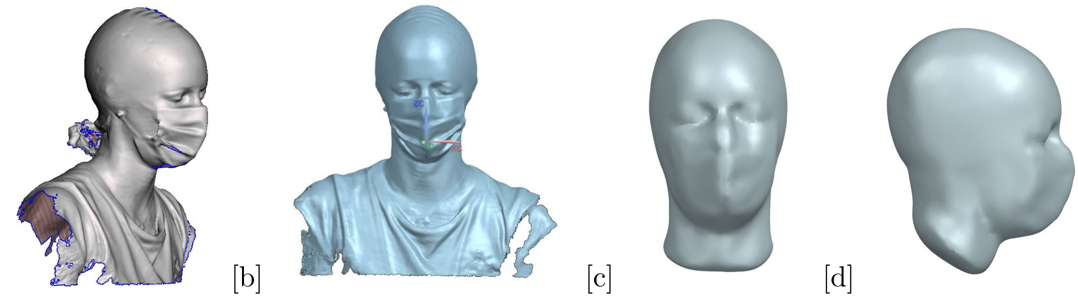

[a] [b] [c] [d]

Figure 3.1: Sequence of 3D head scan: 3D scanner acquisition [a], scan after reparation with Meshmixer [b], solid scan: vision frontal and lateral [c] [d]

[b] is bigger than 105° (as defined by the Standard), while the degree in the subfigure [c] is 25°. By defining the construction lines to be respected of the helmet,it was necessary to draw the design of the surface, not using the software *NX*, but changing with *Rhinoceros* to create a SubD or SubDivision surface.

3.2 Helmet design

3.2.1 Rhinoceros - Helmet surface

After realizing a 'clean', Wang et al. [30] subdivide with lines, and then sectors, the head to create the surface of the helmet. They used the technique of NURBS, a *Non Uniform Rational Basis-Splines*, which mathematically models a 3D geometry while, thanks to the Rhinoceros, 3D organic shapes was draw SubD surfaces. These geometries allow to split the mesh into small polygons and consist of lines with which, easily, the shape of the object can be modified; with a surface already created, changing the position of a line, automatically the remaining part of the geometry adapts to the changes. With this technique, the 'surface base' of the helmet was realized with the size of my head. The representation of the realized SubD is in Figure 3.3.

3.2.2 Grasshopper - Helmet structure

The next idea is the creation on the surface of the beetle structure with different dimensions modelling the helmet that is not a linear surface. It was decided not to build the structure with a software CAD because to model an already complex structure on a curved surface would mean to model a cell for a cell.

To solve this obstacle, a Rhinoceros plug-in was used, *Grasshopper*, GH, idealized by Robert McNeel and associates, creators of Rhinoceros. Using GH does not mean drawing geometries by connecting points and drawing tools because it is based on algorithmic modelling used in architecture and engineering for 3D modelling.

The modelling takes place through a node diagram that the software will convert into a code-algorithm; in GH, it is possible to define the variables and parameters, and in Rhinoceros, in real-time, it is possible to view the object. GH allows for varying the

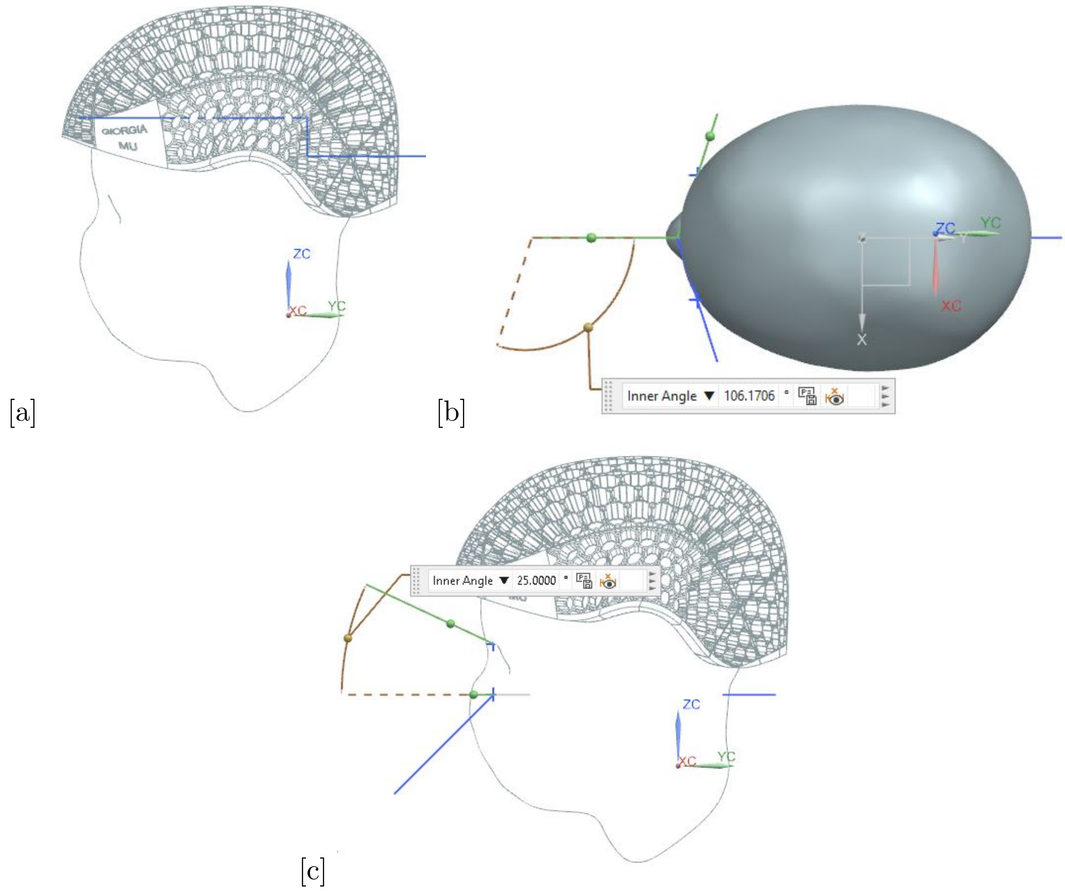

Figure 3.2: Feature's extraction: in [a] is represented the impact line, in [b] and [c] two prospective about the definition of the field of vision

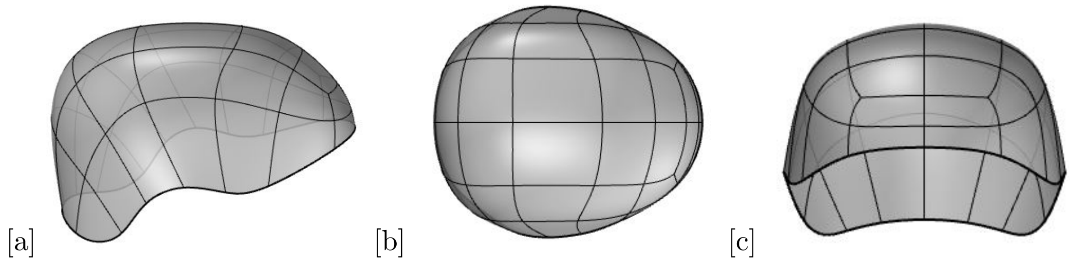

Figure 3.3: SubD representation: lateral view [a], top view [b], front view [c]

geometry to your liking by varying a simple parameter of the diagram, as everything will be remodelled according to the change made.

In the following Figure 3.4 it is shown an example of a structure that was used for distinct subgroups of helmet areas. The idea was to insert smaller cells in the frontal and lateral zone and larger ones in the upper area. In the first image [a] is shown the part of the helpful diagram to create the beetle structure, to establish the size of the cells, and the extrusion; the second image [b] contains the part of the diagram with which I applied the structure previously created to the SubD.

The structure used to place and adapt the beetle structure to the surface is the *SrfMorph*, while the yellow 'window' that contains numbers serves to select the parts of the surface where to apply the geometry created. In accord with the GH diagram in

[a]
[b]

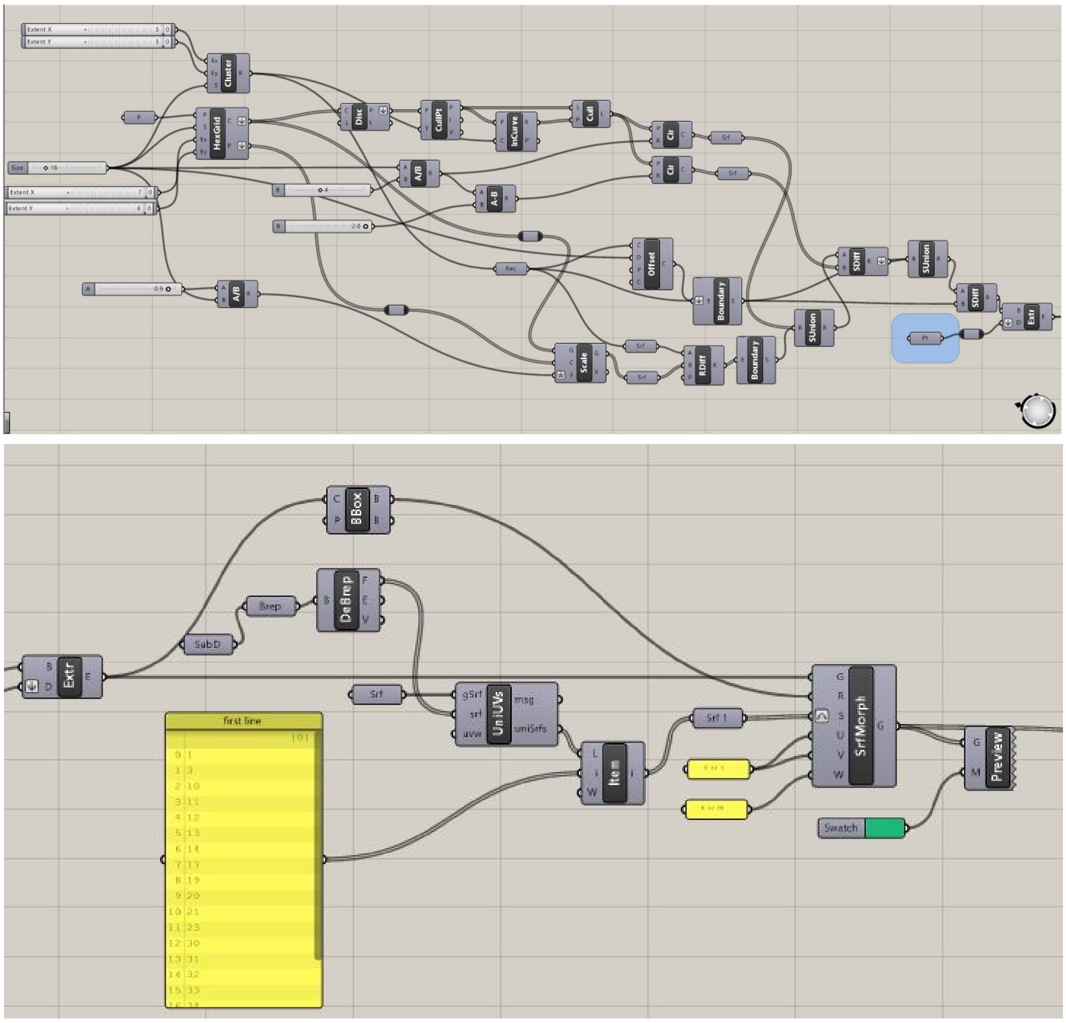

Figure 3.4: Grasshopper diagrams

Figure 3.4 [a], it is possible to see the steps executed to realize the structure. Initially, in the xy-plane a hexagonal grid was drawn through the *Hexgrid* command, in which you can input the length of the hexagon edge and the number of grid elements (selected by trial). Then the circumferences was drawn in proportion to the hexagon dimensions as specified in the Chapter 2 and shown in Figure 3.5 [a]. In figure [b], the 'cut' made at the circumferences is visible; this subdivision was necessary for printing purposes. In the last photo [c], the structure highlighted in green in [b] was extruded, setting a distance of 20 mm.

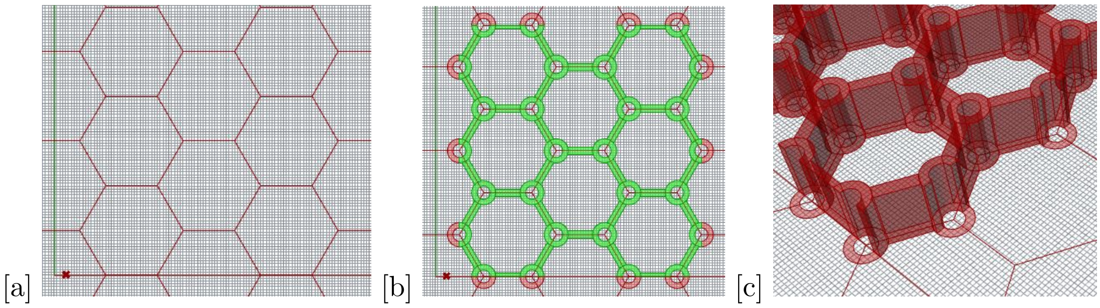

Figure 3.5: Construction sequence of the geometry of the helmet

In the diagram in Figure 3.4 [b], there is the application of the structure created bi-dimensionally to the SubD surface of the helmet, visible by unlocking the *SubD* command of the diagram and in Figure 3.6 [a]. Upper this, the referential geometry of the group of surfaces was superimposed where it was to be applied the newly created structure (visible in darker red); the SubD indices are in the yellow box of the diagram.

Through the *SrfMorph* command, the location of the structure was granted. In Figure 3.6 [b], at the darkest red of the figure [a], with the above command it was possible to place the structure.

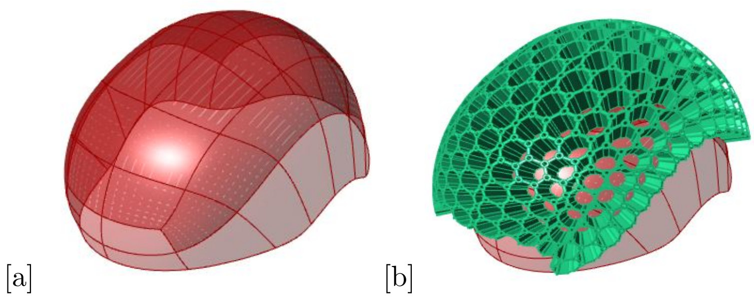

Figure 3.6: Application of the geometry created to the helmet surface

Overall the diagrams with specific structures are five: one for the front, two equal for the side parts, one for the top shown in the previous Figure 3.6 and one for the back.

The hexagons in the structure have a dimension varying between 8 mm and 14 mm of side: the largest is found at the top, later at the back, in the sides, and the smallest at the front. In Figure 3.6 [b], the presence of not only hexagonal structures is visible. The geometry used does not allow the homogeneous arrangement on the entire surface and requires different structures. Automatically the choice of GH to optimize the structure was to insert quadrilateral.

As described above the helmet has different dimensions of the structure, divided as visible in Figure 3.6 in a quadrilateral. This causes a discontinuity between zones with different sizes due to the geometry of the construction.

To eliminate this problem and realize the design homogeneous, grids were inserted in the affected areas, as shown in Figure 3.7. This insertion, however, proved to be interesting and strategic; researching in this regard, studies were realized to demonstrate the insertion of a rectangular grid inside the hexagon grid was helpful for the transmission of stress in the structure. As cited by Sun et al. [40] ”the mechanical properties of these sandwich structures are often limited by local failures such as face-core debonding or core collapse”. Carrying out compression tests have effectively demonstrated that the insertion of the grid allows ”provided increased stiffness, specific stiffness, energy absorption, and critical load” [41]. As shown in the graphic [c] of the Figure 3.7, the honeycomb structure gives a force of 7 kN, while, with a grid, the value is 11 kN and with the combination exceeds 22 kN. In addition, in the left front, a plaque to customize the helmet was prepared, Figure 3.7 [a].

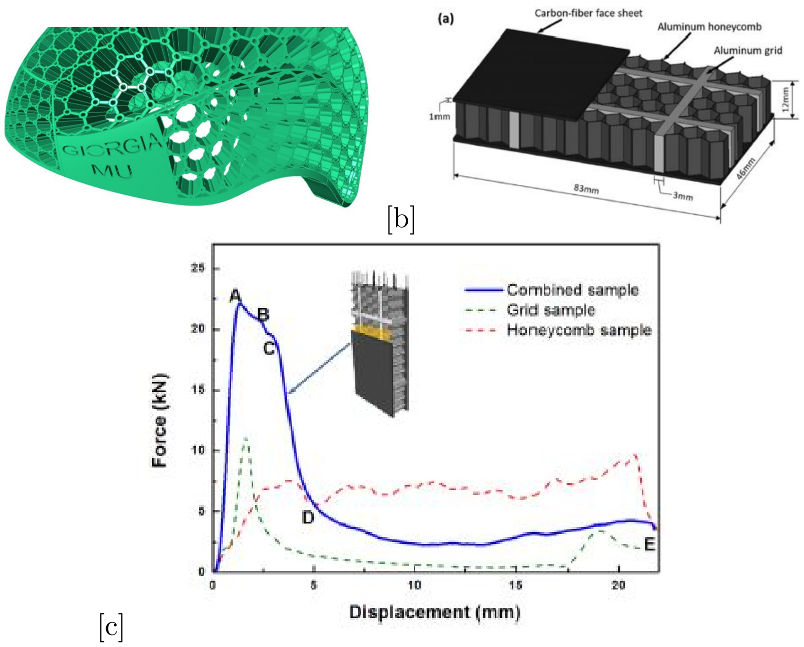

[a] [b] [c]

Figure 3.7: Grid in the helmet [a], hybrid structure with hexagons and grid [b] [40], compression test results of the hybrid structure [c] [41]

3.3 3D Print

After having achieved the CAD (Computer Aided Design) of the helmet, in order to be printed, it must be converted and saved in format .STL (Standard Triangulation Language) - Binary, compatible with the printing machine and useful for transforming solid object surfaces into triangles. The steps to be taken are the following:

- CAD file realization;
- CAD export in format .STL to Simplify 3D, the software that shows slider layers, and then:
  - rotate and position the object according to geometry and the positioning of any

supports;
- setting printing parameters;
- item manual and/or automatic positioning of supports;
- slider display layers;

- import file .gcode to printer

3.3.1 Printer and parameters

The program used to visualize how the helmet slices layers before sending it to the printer and to set the parameters is, as anticipated, *Simplify 3D*.

To make the printing not being a flat geometry, it is necessary to place the supports. The idea was to use water-based supports that the helmet would automatically dissolve once placed in the water. After testing different types of water-soluble PVA, the choice fell on *eSun 3D Printing Filament PVA* (water-soluble support). Before choosing the optimal position for printing, several tests were carried out and, to decrease the number of the supports significantly and allows an optimal printing of the outer part; an empty 'sphere' that self-sustains below the helmet was placed, as shown in Figure 3.8.

In the image [a] you can see the first print position tried, with which an external part of the helmet very damaged was obtained because of the contact supports-helmet. In [b] the empty 'sphere' is shown to optimize the number of supports and in the last photo [c] there is the full version at the end of print.

[a] [b] [c]
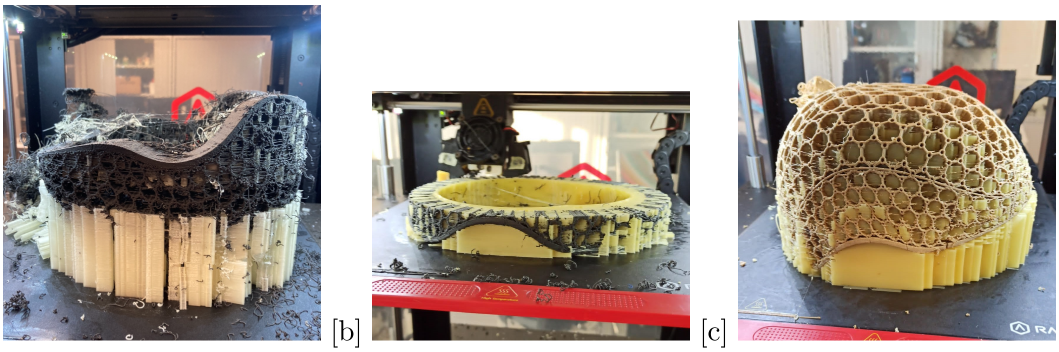

Figure 3.8: Printing supports

The printer that has been used for printing is the *Raise 3D Pro2*, with double extruders and nozzles of variable size from 0,2 mm to 1 mm; after some test prints with the PLA LW and the structure in created, the size that allowed me to have a good compromise between printing time and accuracy was 0,6 mm. Using 0,4 mm, the printing time was excessive, even if having the smaller nozzle diameter means having more precision; with the 0,8 mm nozzle, the quality of the structure was not excellent, as seen in Figure 3.8 [a].

Another factor that had to be taken into account is the characteristic of the PLA-LW to expand. As the printing temperature and the printer used vary the expansion and characteristics of the material change. The use of the **0,6 mm** nozzle associated with

Parameter	Left extruder	Right extruder
0.1cm Material	0.1cm PVA	0.1cm PLA LW
Extruder toolbox index	Tool 0	Tool 1
Nozzle diameter	0,6 mm	0,6 mm
Extrusion multiplier	1	0,5
Extrusion width	Auto (0,72 mm)	0,5 mm
Layer	x	
Infill		Rectilinear - 50%
Supports (Automatic and not)	Infill 50%	
Temperature	210°	250°

General parameters

Primary layer height	0,3 mm	Top solid layer	4
Bottom solid layer	2	Outline	2
Heated bad	60°	Speed	40 mm/s

Table 3.1: Printing parameters

Raise 3D allowed me to get good results. The choice of this printer was not random, it has in fact the characteristic of making extremely precise prints. The Raise has accuracy in placing the object on the printing bed of 0,78 microns on the x/y axis and a resolution for layers of 0,01 mm.

The final version of the helmet is visible in Figure 3.9 and it is possible to compare it with the preview version in Rhinoceros, in Figure 3.10.

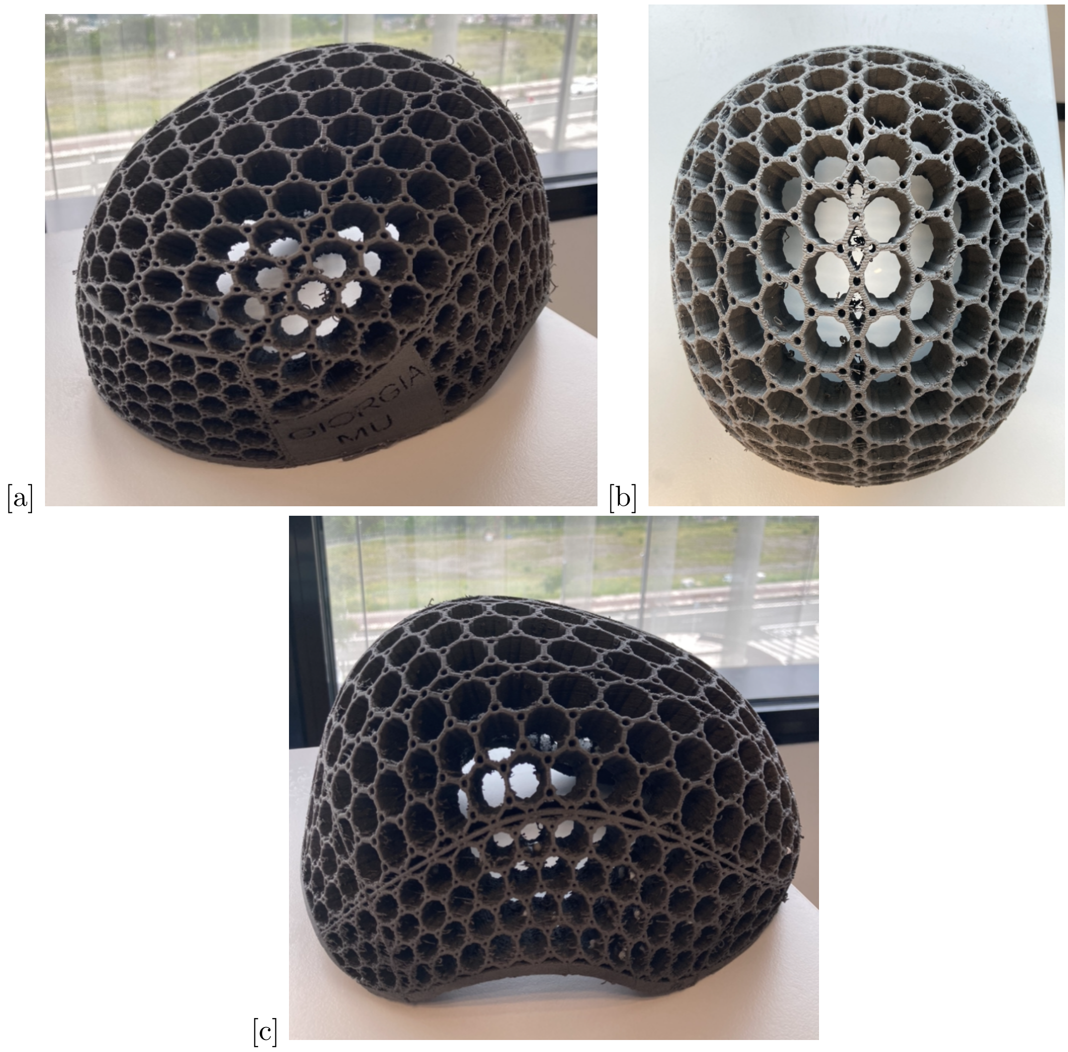

Figure 3.9: Views of the helmet

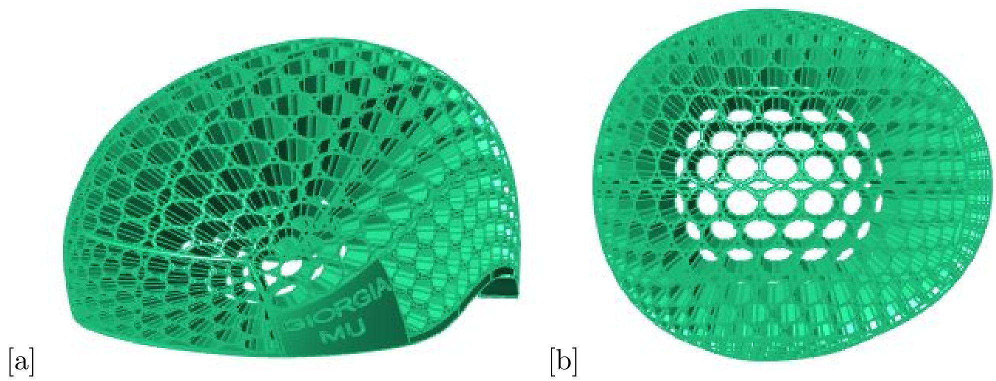

Figure 3.10: Views of the helmet (GH version)

Chapter 4

Experimental evaluation

4.1 Experimental tests

4.1.1 Drop-weight impact test machine

In order to calculate the contact force peak and the difference of energy absorbed during the impact between the reference helmet and helmet with the beetle structure in PLA-LW, dynamic impact tests were carried out using the *Fractovis Plus*, an impact test machine.

In this way, it is possible to monitor the evolution of the above variables from the initial to the final instant of the impact. The machine can withstand a load with a range variable from 2 to 70 kg, with a maximum speed of 4,6 m/s and a maximum height of 1 m. The values chosen for the test are the following: 5 kg weight, maximum speed and maximum height. The Anvil that was used is a disc diameter of 60 mm.

As shown in Figure 4.1 and explained by Crupi et al. [37], the machine consists of a sensor capable of recording the speed before impact, the impactor that can have a variable mass (a weight of 5 kg in my test), a system to guarantee that there are no multiple impacts after the first and that work as a shock absorber and clamping system where the object to be tested is placed.

The tests that have been carried out are in total four: two related to the helmet optimized with PLA-LW and two with two generic helmets of different brand in EPS.

4.2 PLA LW helmet

To perform the dynamic test on the helmet of PLA, considering the difficulty of printing, it was helpful to use a test helmet with imperfections to understand where the impact was concentrated in a single part or distributed. The images of Figure 4.2 show a helmet with not well defined edges and inaccurate print, but exactly localizes the impact zone. Thanks to this test it was possible to take into account only one helmet area, shown in Figure 4.3, to have the exact curve of the structure bio-inspired with PLA-LW.

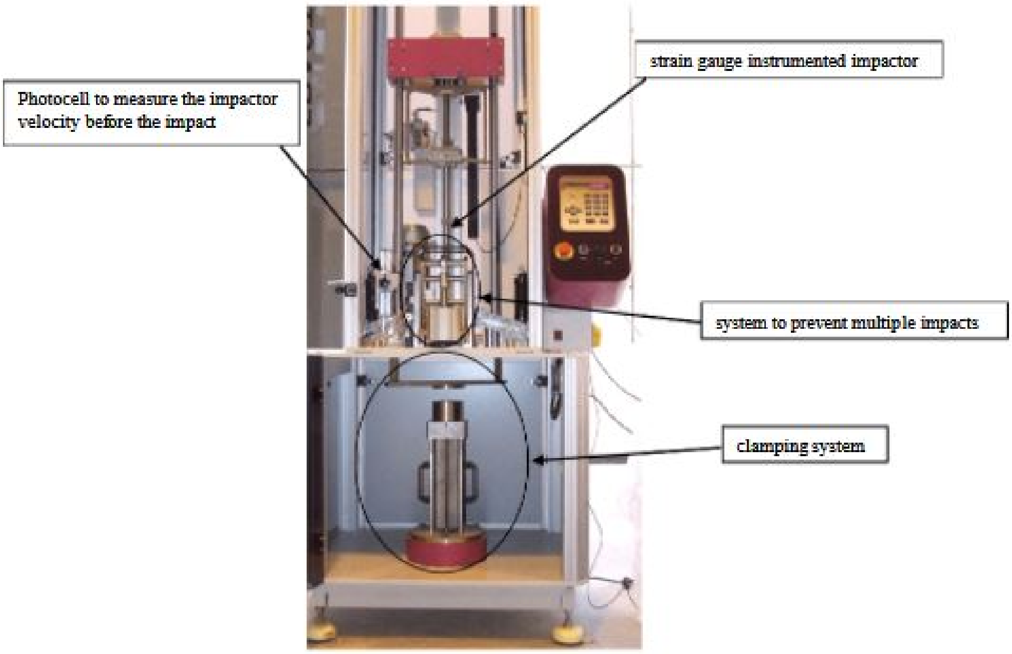

Figure 4.1: Drop-weight impact test machine [37]

[a] 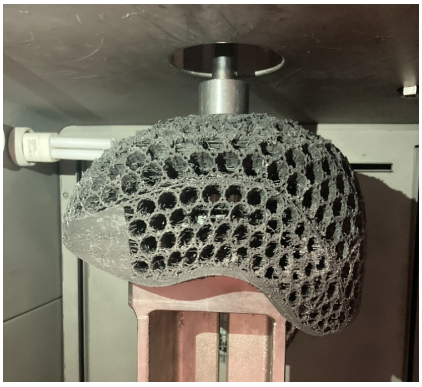 [b] 

Figure 4.2: Test 1: PLA-LW helmet

4.3 EPS helmet

To carry out dynamic tests and extract the technical characteristics of the helmet,two helmets were bought in a sports store, both EPS and, being on the market, both certified. The brands of the two helmets are: DTB and VAN|RYSEL, and the average weight of the two is 223 g. Two different helmets have been chosen to have a more certain and clear classification of the characteristics. They are shown in Figure 4.4 and Figure 4.5.

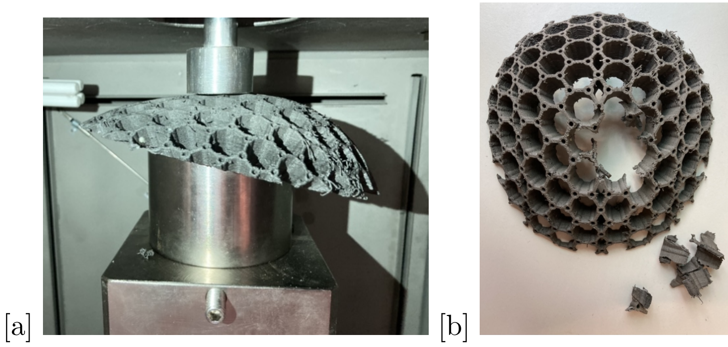

Figure 4.3: Test 2: PLA-LW helmet

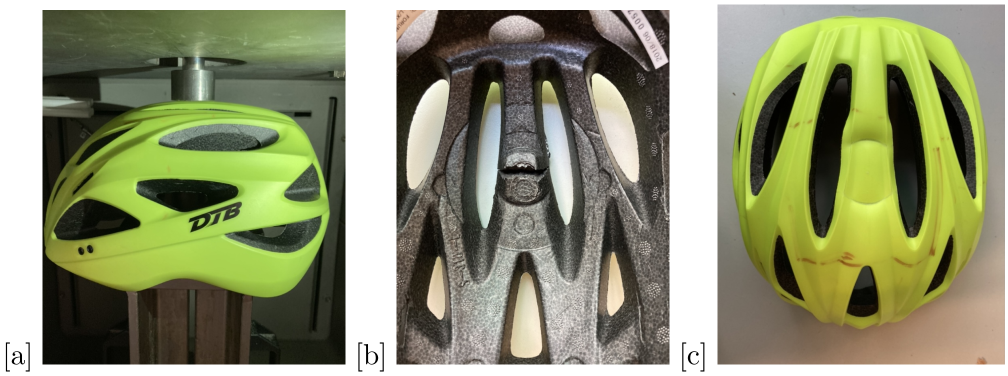

Figure 4.4: Test 3: EPS helmet

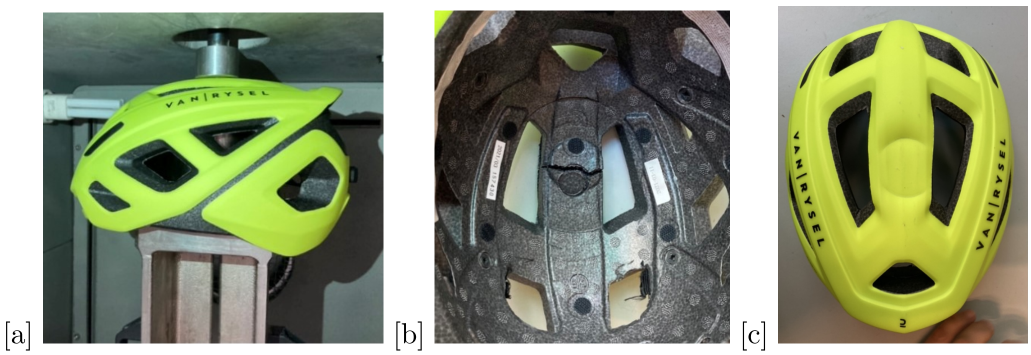

Figure 4.5: Test 4: EPS helmet

4.4 Results

4.4.1 First results - PLA-LW and EPS helmet

Figure 4.6 shows two types of trends related to the two different models of the helmet. The force evaluated for PLA-LW has higher force peaks but is more concentrated and propagates less than EPS. The graph shows the peaks of each curve, highlighted with a red circle. In tests 1 and 2 for the PLA-LW as mentioned earlier, the values are higher, about 7301 N for the complete helmet and 3996 N for the portion of helmet. This difference is due to the inaccuracy of the first full helmet during the printing phase. In Figure 4.2, it is visible the low homogeneity and precision. Therefore the first test with full helmet was used only to define the area of interest of the impact, which turns out to be localized. For the other two EPS curves, the values are only slightly lower compared to the PLA-LW, equal to 3620 N and 3295 N, but the trend is much more distributed.

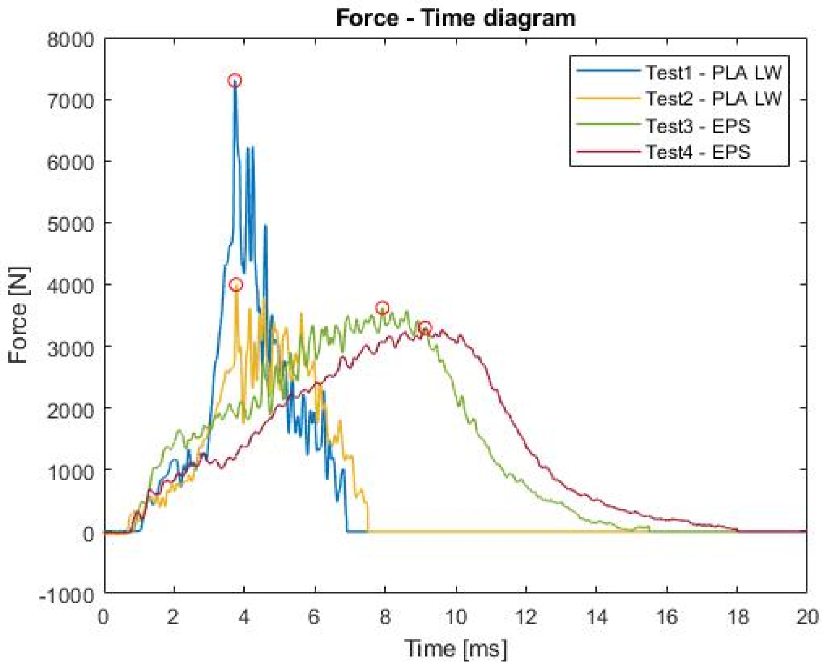

Figure 4.6: Dynamic machine test - Force

With the data obtained from the impact machine, it was possible calculate not exclusively the value of force, but it's also possible to view the energy curves. A resume about the values and energy of the force is in the following Table 4.1:

Test	Peak force [N]	Peak energy [J]
Test 1 - PLA LW (inaccurate)	7301.30	
Test 2 - PLA LW (portion of helmet)	3996.43	
Test 3 - EPS (DTB helmet)	3620.07	50.9
Test 4 - EPS (VAN|RYSEL helmet)	3295.46	41.98
Test 5 - PLA with TPU	4542.1	50.22

Table 4.1: Energy absorbed in dynamic test

4.4.2 PLA-LW helmet with TPU cover

As it is possible to see in Figure 4.7 and as highlighted, the first tests concerning the bio-inspired structure and the PLA-LW are far from my expectations, considering the little distribution of force in comparison with the EPS foam, and, consequently, a small amount of energy absorbed.

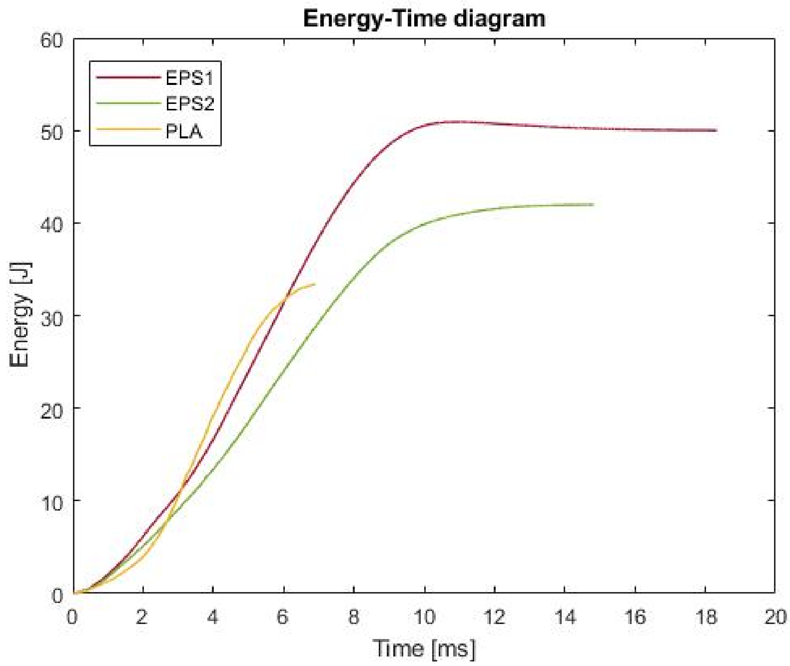

Figure 4.7: Dynamic machine test - Energy

To improve this impact damping factor, the idea was to create a cover for the helmet in flexible TPU, trying to absorb impact energy. The TPU used is a flexible material of the brand *Ninjaflex*, used in sports by the application in helmets and shoes, to cushion bumps during the game. Generally, in the helmets (baseball helmet, for example), the TPU is inserted internally in contact with the head. In my case, the TPU structure, in addition to creating a shock-absorbing and durable cover, creates a custom cover the helmet and for the person. This cover was also made with the Raise 3D printer.

As shown in the Figure 4.8 [a] the infill of the part in contact with the helmet has a percentage of 100%, the filling of the other part of the structure is not complete, but only 15% and the internal structure is hexagonal to recall that of the helmet. The desire to insert a structure with a 'raised' geometry is for visual and aesthetic reasons, as you have the feeling of greater protection and not filled is inspired by the machine *Citroen Captus*, whose bumpers (*Airbump*) are full of air. The failure to realize empty structures is due to the need to place any internal supports not removable.

The idea was to create a cover that allow you to see of the internal structure of the helmet and that protect specific areas: the front, the two sides, the top and the posterior. What which was thought, for this reason, was to create the shape of a flower with four petals, Figure 4.8 [b].

In this way, to perform dynamic impact tests as shown in Figure 4.9 [a], the cover was positioned at the top of the helmet, and the impact was performed in the centre of the 'flower', which corresponds to the higher upper part where the structure has larger cell size. The impact parameters are the same as those used in previous impacts: 5 kg weight, maximum speed and maximum height. The Anvil that was used is a disc diameter of 60 mm. In photo [b], it is evident the difference between the structure that received the impact with protection (left) and without protection (right). Without protection during the impact, there was a perforation of the structure with a concentration of force at a local level as you can see in the Figure 4.6; in the case of TPU the impactor did not perforate and crossed the structure, thanks to the cover of TPU that cushioned the shock. At the moment of impact, the impactor bounced.

[a] [b]

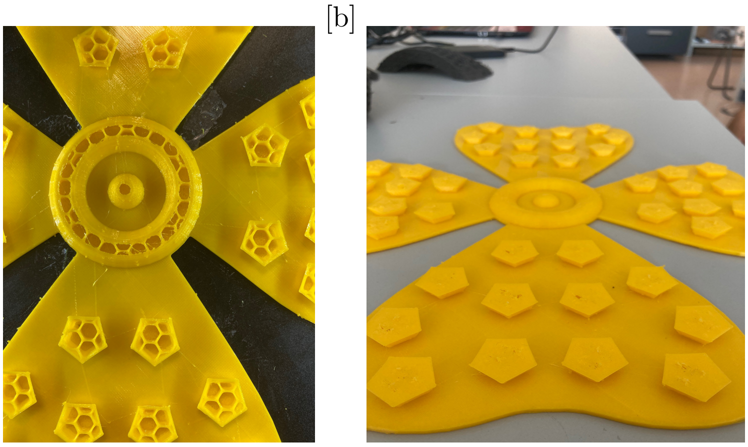

Figure 4.8: TPU cover

[a] [b]

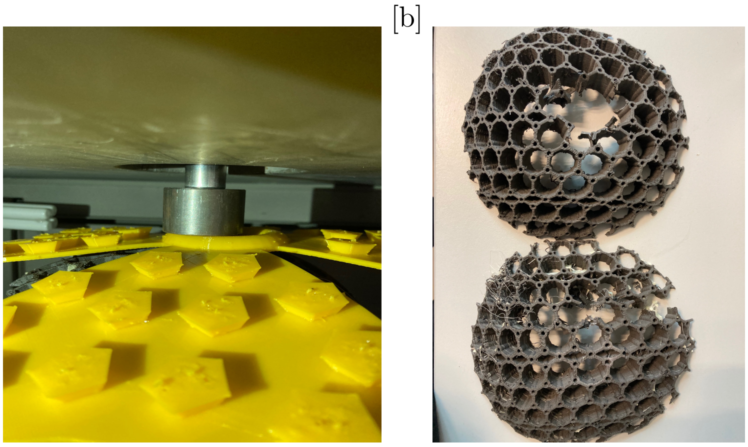

Figure 4.9: PLA-LW with TPU - dynamic impact [a] and differences between the helmet with TPU and without TPU cover [b]

The Figure 4.10 includes the diagrams relative to the dynamic impacts. In [a] there are already analyzed EPS results, in [b] a comparison between the test on the portion of helmet in PLA LW with and without the TPU cover, in [c] the overall comparison of curves shows a much more similar EPS trend if the TPU is placed above the structure in PLA LW, to soften the blow and absorb the same energy [d].

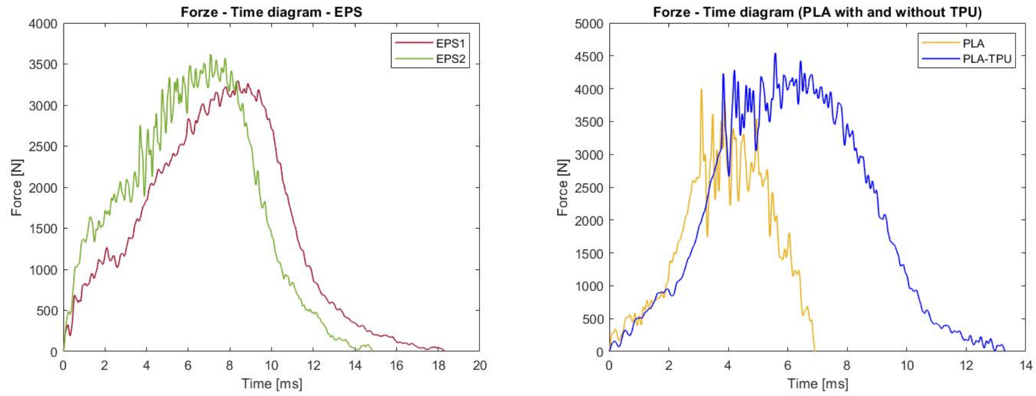

[a]

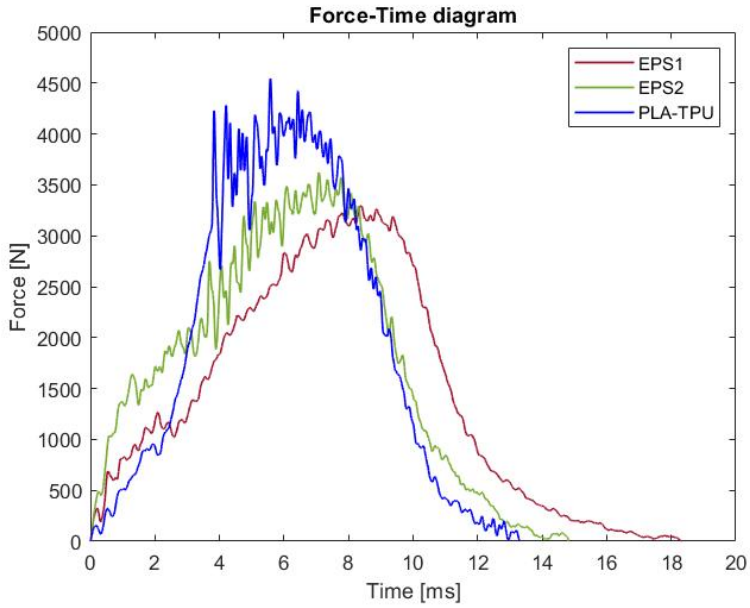

[c]

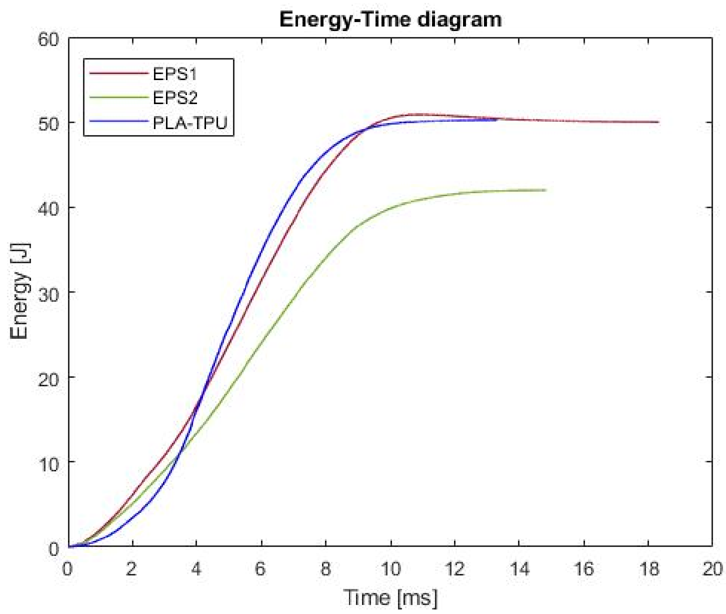

[d]

Figure 4.10: Comparison between PLA-LW with TPU and EPS

Chapter 5

FEM Validation

5.1 Impactor - Anvils definition

Before to start to work in Abaqus, it was necessary to search in the literature the material with which the anvil was been realized. Milne et al. [23] established the density's value, the Young's Module and Poisson's ratio for the Flat and Kerbstone Anvil.

- Density ρ = 7800 kg/m^3
- Young's Module E = 200000 MPa
- Poisson's ratio ν = 0,3

Inserting the data in the CES EduPack program, specifying the mechanical and physical properties, the material corresponding to these characteristics is Stainless steel, austenitic (ASTM F1586), medium-hard.

Initially, the proposal was to create a conservative system to evaluate the absorption energies values and apply this value to a vibration system, but the helmet needs damping to be realized; it was impossible to use a system without losses in this modality. This is why a numerical calculation was carried out by performing two types of simulations: explicit dynamic step and static step.

The idea to realize the theoretical impact is to regard the movement of the anvil and not the helmet's movement, which is fixed. The velocity is the same cited in the normative EN 1078, 5,42 m/s for the Flat anvil and 4,57 m/s for the Kerbstone anvil.

In performing the simulations, It was given more relevance and perform tests with the Kerbstone Anvil. This choice was done because the geometry with which it is been realized (following as defined in the legislation) allows the helmet to be more subjected to stress; this involves the definition of higher stress limits compared to the Flat Anvil.

The mesh size that has been used is the same in the case of the simulation of the helmet optimized in PLA-LW and the full helmet in EPS, of 7 mm. The impactor is considered as a *Discrete rigid body* with its specific Reference Point (RP) like shown in Figure 5.1; for this reason, it is not a solid, but it is compusted only by shells. In the same image [b], there is the FEM representation of the model and in Table 5.1 the characteristic of FEM, with quadrilateral (R3D4) and triangular elements (R3D3).

Object	Element number	Elements Shape	Geometric order	Global size [mm]
Kerbstone	230	Quadrilateral - R3D4	Linear	7
Kerbstone	8	Triangular - R3D3	Linear	7

Table 5.1: Mesh element - Kerbstone Anvil

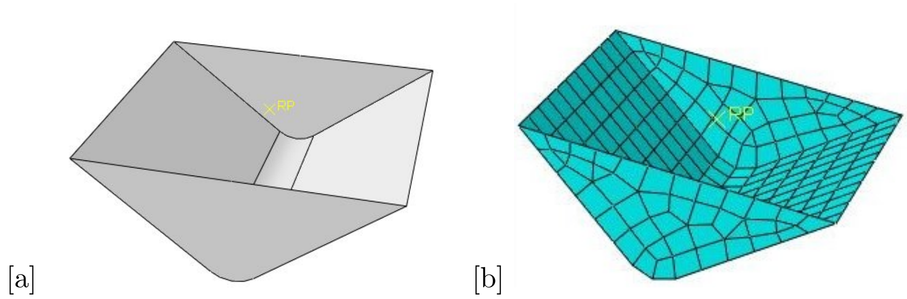

Figure 5.1: Kerbstone anvil in the simulation like discrete rigid body [a] and FEM elements [b]

5.1.1 PLA LW - Plastic characteristics

The PLA-LW, as explained in the Chapter 2, is new material on the market and produced by the only Colorfabb company; for this reason, few tests have been carried out to define its technical characteristics and, through tensile tests of the 3D printed specimens, it was possible to define an elastic limit as reported in the Table 2.10.

In the context of simulations, to reproduce the impact and deformation of the helmet, is also necessary to consider the plastic characteristics of the material. Not possessing any reference value in this regard, tests were performed through a Static Step initially and then an Explicit Dynamic Step in Abaqus.

The structure chosen to consider as a reference it is one of the structures previously subjected to the compression test, having the side L=14 mm. As for the reproduction of the compression disks, initially they were reproduced according to the geometry of the Hoytom HM-D Testing Machine, considering the bodies mentioned above as discrete 3D rigid discrete. The measure was the diameter of 200 mm and the height of 20 mm.

After an initial analysis, it was observed that the computational time of the simulation program was very high, so it was decided to change the geometry to have a 'disk-surfaces' (equally 3D rigid-discrete) which allowed me to have a smaller number of nodes for the mesh and, consequently, a better computational time. The representation of the optimized structure in PLA-LW and the disks used for simulated compression is in Figure 5.2.

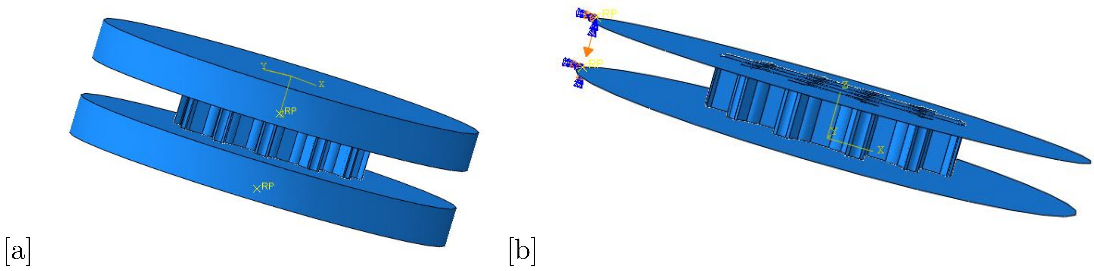

[a] [b]

Figure 5.2: Representation of the samples used for the simulation of the compression test. In Figure [a] the disks of the Hoytom HM-D Testing Machine, in figure [b] the representation of the same as simple surfaces

As shown in Figure 5.2, the disks are considered 3D discrete hard bodies, so it was chosen for both a point, the reference point RP, where to apply the characteristics related to the two bodies. As for the compression test, it was established:

- the movement of a disk and fixed the second through a boundary condition, imposing an Encastre, therefore unable to move and rotate in x,y,z directions;
- for the opposite disk the boundary condition relative to the 15 mm displacement was applied, which is the parameter that it was observed to determine the end of the compression with the machine. This shift is shown by the orange arrow in figure [b];
- between the upper surface and the disk e the disk with the lower surface it was initialized a general contact with normal behaviour through 'hard' contact and tangential behaviour with a coefficient of friction of 0,2; with directionality imposed on 'isotropic'.

The next step was to define the mesh of the components, whose parameters are shown in Table 5.2, while the representation of the FEM is in Figure 5.3 with the representation of the simulation and real compression test.

Object	**Elements number**	**Typology**	**Geometric order**	**Global size [mm]**
Disk (14mm)	80910	hexaedral - C3D8R	Linear	0,7
Impact disks	206	quadrilateral - R3D4	Linear	20
Impact disks	6	triangular - R3D3	Linear	20

Table 5.2: Mesh element - Compression test simulation

As previously announced, a static simulation was initially performed with a Static Step, with Step Time equal to 900 (obtained going to consider the speed of 1 mm/min of

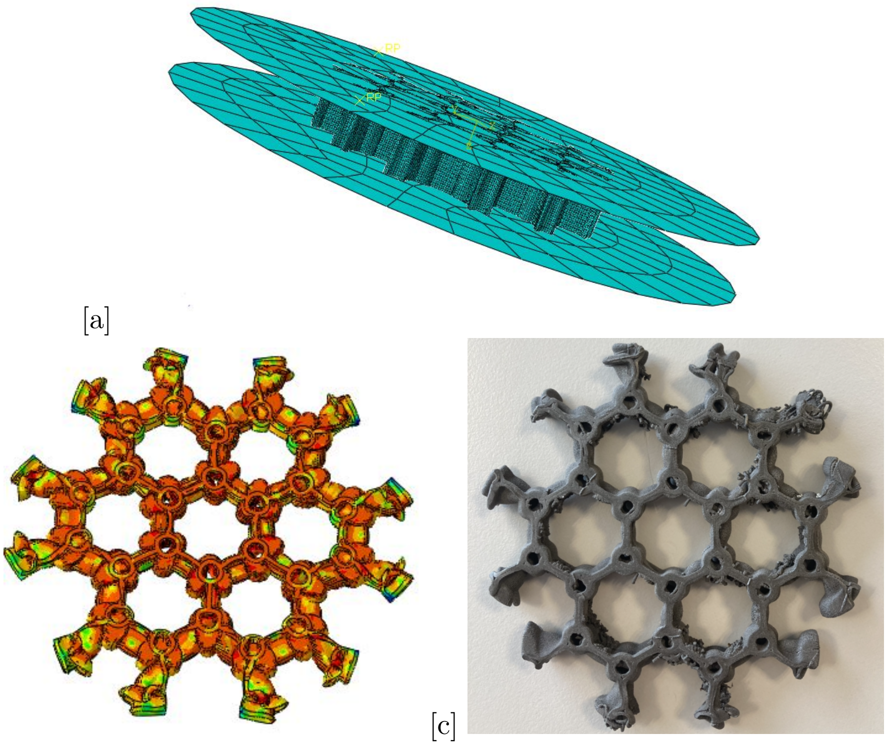

[a]

[b] [c]

Figure 5.3: FEM representation [a] and compression test simulation [b] and real compression [c]

the compression test and the displacement of 15 mm). However, the complex geometry of the structure and the high time set by Step Time, did not allow a correct definition of the parameters of the plastic characteristics of the material; the simulation was not able to continue once reached a Step Time of, approximately, 220. That is why it was changed by choosing an Explicit Dynamic step.

Leaving all the parameters of the boundary conditions unchanged, the Step Time was modified, imposing it to 0.01. The ability of the explicit dynamic to work with non-linear and contacting structures allowed me to achieve results. The results obtained are shown in Figure 5.4 with the blue curve and were obtained through the iteration of different Plastic Strain and Yield Stress values in Abaqus, while the red line is the result of the real compression test; a similar curve trend was obtained, but it is not possible to obtain the same curve taking into account problems of printing inaccuracy.

5.1.2 First test - helmet

The initial idea was to perform a simulation imposing the speed of 4,57 m/s to the impactor, tie the helmet in EPS and PLA, and compare the absorbed energies. The problem it was encountered is related to the mesh of the helmet optimized in PLA, and with minimum dimensions of the elements and distinct elements, it was not able to solve it.

[a]

.	Yield Stress	Plastic Strain
1	4,7	0
2	7	0,01
3	7,5	0,05
4	10	0,1
5	10,8	1
6	11,5	1,5
7	12	2

[b]

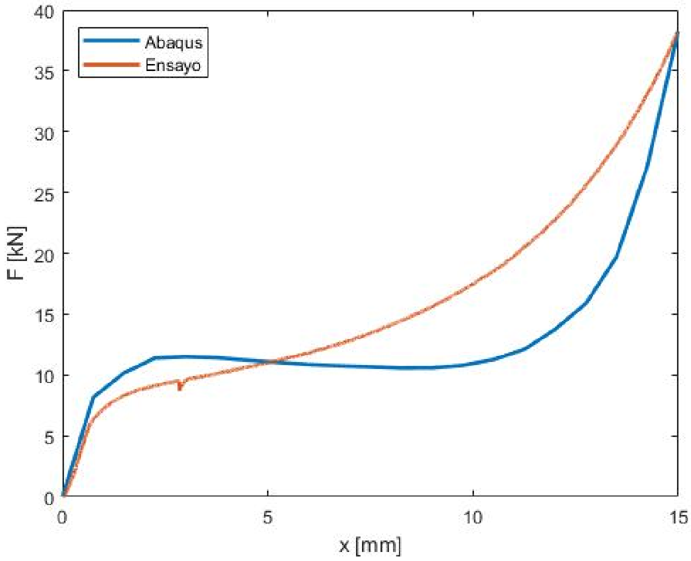

Figure 5.4: Representation of the two curves related to the simulation in Abaqus of the compression test and the data obtained from the real test to obtain the plastic characteristics of the material

5.1.3 Second test - plane

The first solution is the one shown in Figure 5.5. To realize the simulation it was realized a section of the helmet to involve a smaller number of elements and nodes. Again, the simulation for the EPS helmet was successful, while the simulation with the bio-inspired structure was interrupted by excessive distortion of elements.

The previous images show the impact is very localized in the impacted area, and the idea to achieve a complete simulation is not to consider a curved portion of the helmet but a plane. In this way, it was possible to solve the problem and obtain a complete simulation for the bio-inspired structure.

FEM element

Below, in Table 5.3, there is the definition of the elements used for the PLA-LW and EPS plane in the simulation to simulate the impact and to control the energy-absorbing, while the anvil characteristics are described in Table 5.1.

5.1.4 EPS impact simulations

In order to proceed with the simulation, it was imposed some boundary conditions that regard ties and forces;

- the movement of the plane is fixed through an Encastre, therefore unable to move and rotate in x,y,z directions;

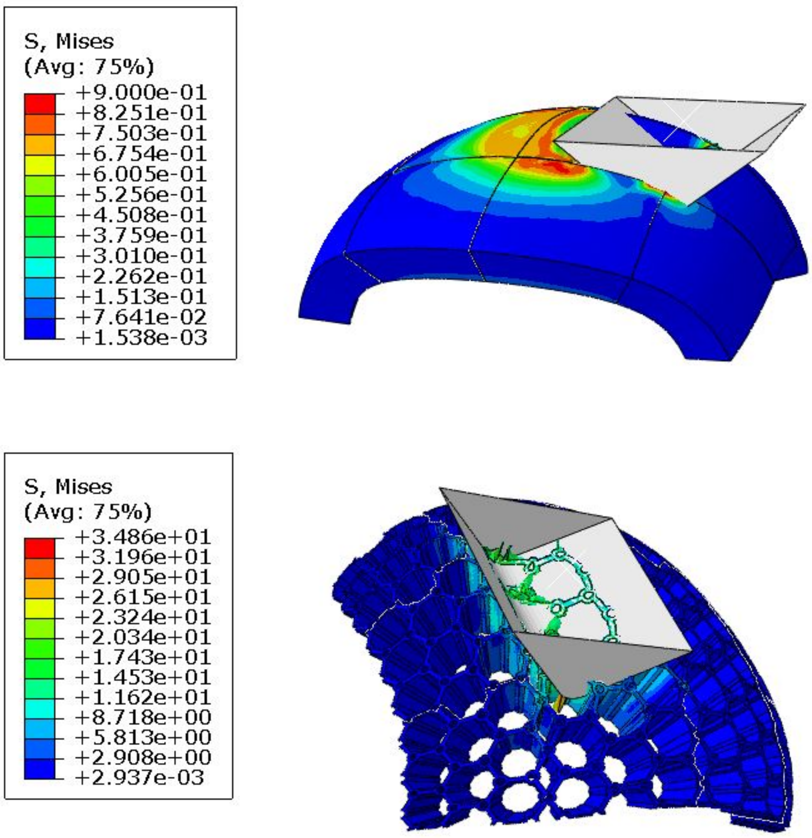

[a]

[b]

Figure 5.5: Impact simulation: parts of EPS and PLA helmet

Object	**Element number**	**Elements Shape**	**Geometric order**
Plane (PLA)	38896	Tetrahedral - C3D10M	Quadratic
Plane (EPS)	2100	Hexahedral - C3D8R	Linear

Table 5.3: Mesh element - plane impact

- to create the impact it was set a speed of 4,57 m/s at the reference point RP of the rigid body, which is the impactor Kerbstone Anvil shown in Figure 5.6;
- between the upper surface of the plane and the impactor it was initialized a Surface to Surface contact with normal behaviour through 'hard' contact and tangential behaviour with a coefficient of friction of 0,2; with directionality imposed on 'isotropic';
- the rotation in x, y, z relative to the RP of the rigid discrete impactor body is locked

In addition, it was characterized the plane in the part of the materials with the characteristic values of the EPS mentioned in Chapter 2.2.1. The Von Mises Stress value, apparently low, is relative to the Yield Stress of the EPS material equal to 0,9 MPa.

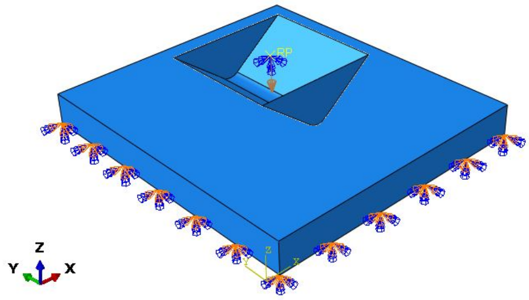

Figure 5.6: EPS: Boundary conditions and Load

5.1.5 PLA LW impact simulations

As also required in the case of the EPS plane, in order to proceed with the simulation some boundary conditions were imposed, that regard ties, and forces;

- the movement of the plane is fixed through an Encastre, therefore unable to move and rotate in x,y,z directions;
- to create the impact a speed of 4,57 m/s was set at the reference point RP of the rigid body which is the impactor Kerbstone Anvil shown in Figure 5.8;
- between the upper surface of the plane and the impactor it was initialized a Surface to Surface contact with normal behaviour through 'hard' contact and tangential behaviour with a coefficient of friction of 0,2; with directionality imposed on 'isotropic';
- the rotation in x, y, z relative to the RP of the rigid discrete impactor body is locked

In addition, the plane was characterized in the part of the materials with the characteristic values of the PLA mentioned in the Chapter 2.2.3 and 5.1.1.

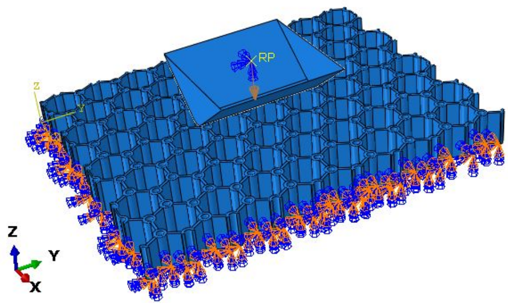

Figure 5.8: Boundary conditions and Load

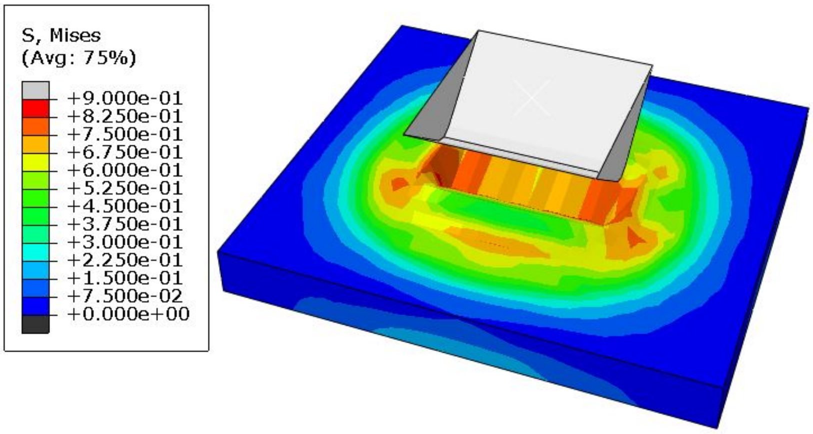

[a]

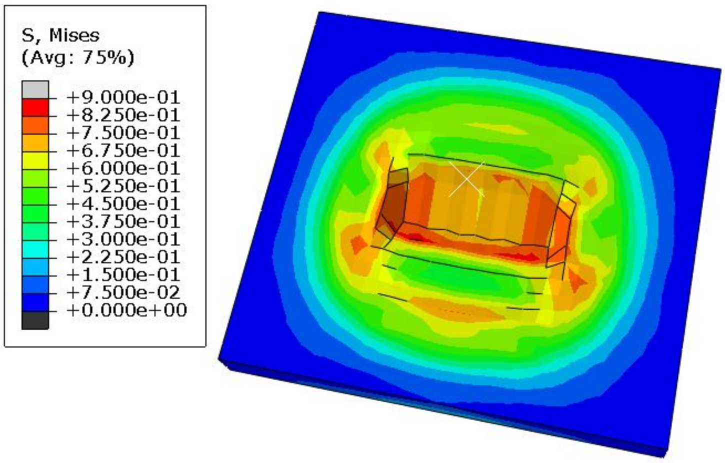

[b]

Figure 5.7: EPS impact simulation

5.2 Results

In Figures 5.9 and 5.7, it is shown how the structure in PLA LW has a more concentrated stress distribution of the structure, unlike EPS. The maximum value for the Von Mises stress is 0,9 MPa in EPS structure, and 36,34 MPa in PLA LW structure. Once the simulations were obtained, the next step was to go and compare the energies absorbed by the two structures. The energy calculated by Abaqus that has been taken into account is Plastic Dissipation. To make a comparison, the data of the two energies were represented in a single graph.

What emerges from the graph is that, about the impact made with the Kerbstone Anvil, the energy absorption is more excellent, although only slightly, for the PLA LW than for the EPS. From the graph, in Figure 5.10 a value of 41 J is shown for the EPS and 51 J for the PLA LW.

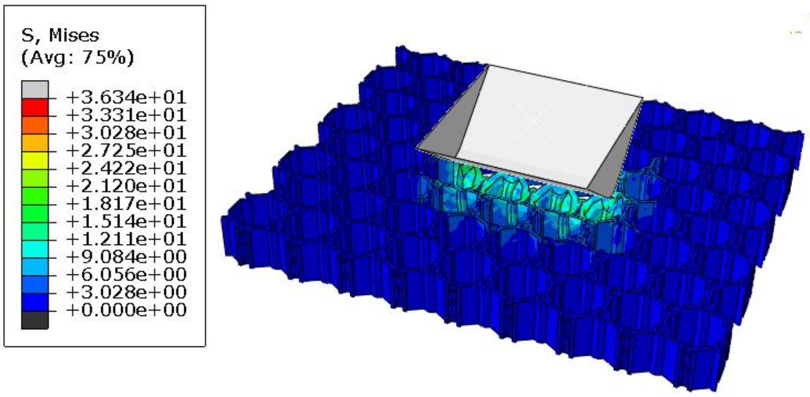

[a]

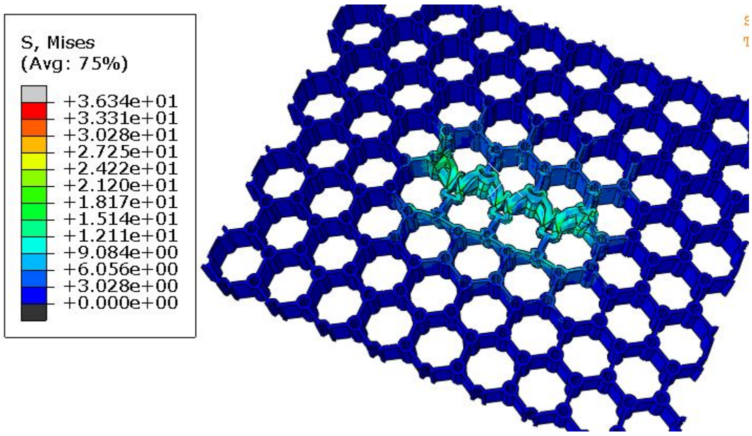

[b]

Figure 5.9: PLA impact simulation

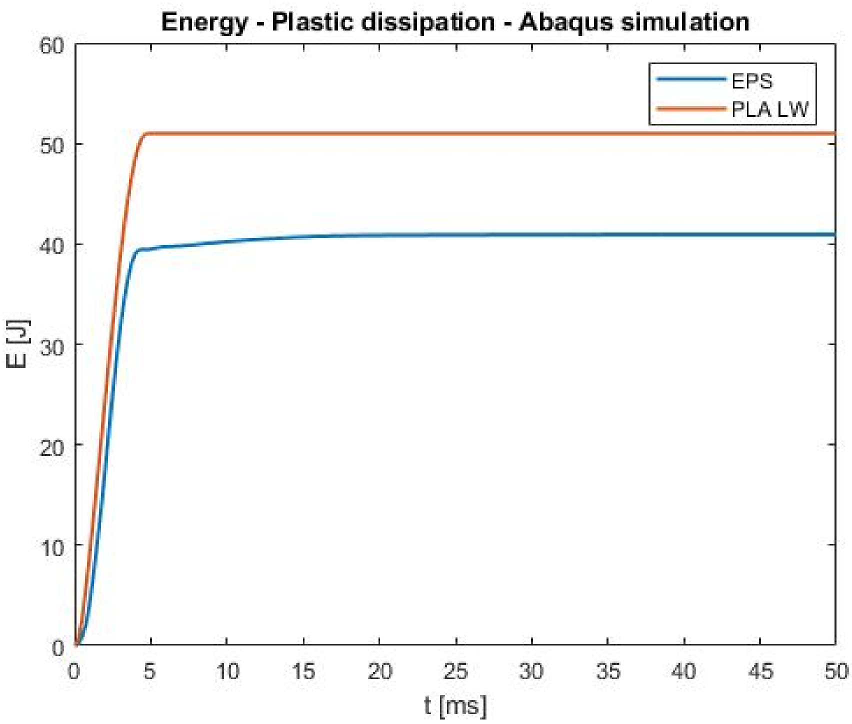

[a]

Figure 5.10: EPS and PLA LW energy comparison - Abaqus simulation

Chapter 6

Head Injury Data

For the statistical analysis the injuries related to the accident data were categorised into the following types and levels based on the details of the medical report [11], about the EN 1078:

- **Head Injury Criterion (HIC)**
- **Peak Linear Acceleration (PLAc)**
- **Gadd Severity Injury (GSI)**
- **Diffuse axonal injuries (DAI)**

6.1 Abaqus simulation

Until now, the purpose of the simulations has been to determine which, between the two materials and the two structures of EPS and PLA LW could absorb more energy during the impact, but no simulations have been carried out in compliance with BS EN 1078 on the helmet impact tests. To calculate the injuries listed in the previous paragraph, however, we need the acceleration values in the three directions related to the subject's head.

To realize it, the scan of my head already 'clean' was considered, of which it has been calculated the inertia thanks to the automatic SolidWorks calculation and evaluated the weight with the Table 2.4, the structure of the helmet was placed for the EPS and the PLA LW over the head as shown in Figure 6.1. Also this time being able to mesh the entire helmet in PLA LW was impossible due to the excessive distortion of some elements during the simulation, so it has been tried to make a section of the structures of the helmet and results were obtained.

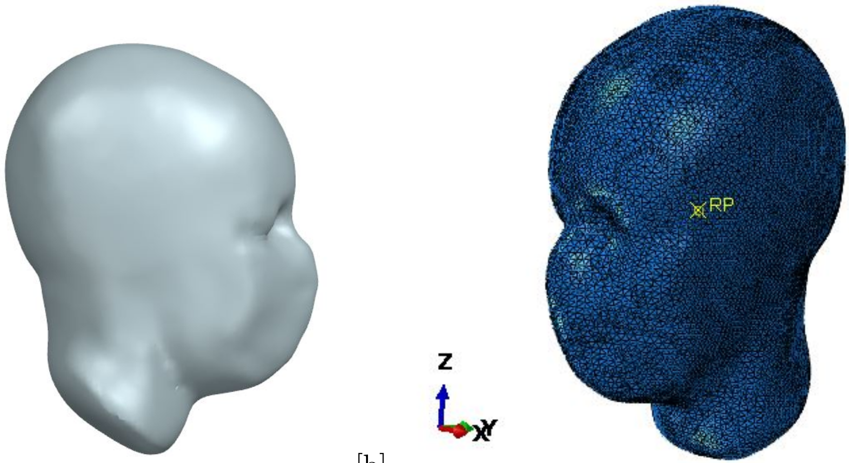

[a] [b]

Figure 6.1: My scan head - CAD [a], head imported in Abaqus[b]

Initially, the simulation had these characteristics, as shown in the following Figure 6.2, considering the helmet was not sectioned. As explained earlier, it was not possible to get to simulation in the case of the optimized structure in PLA LW; for this reason, only a part of the helmet was considered in both cases, shown in Figure 6.3.

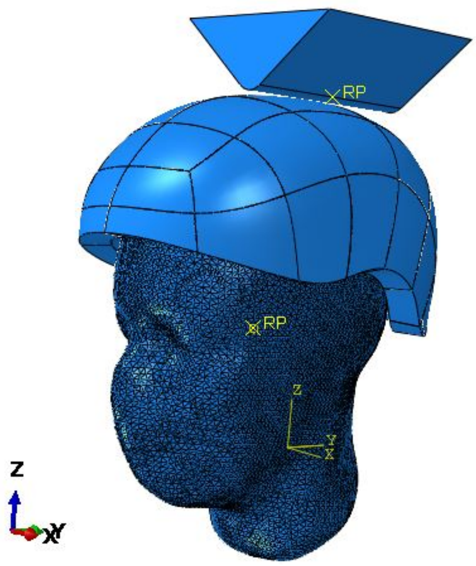

[a]

Figure 6.2: Simulation based on BS EN 1078

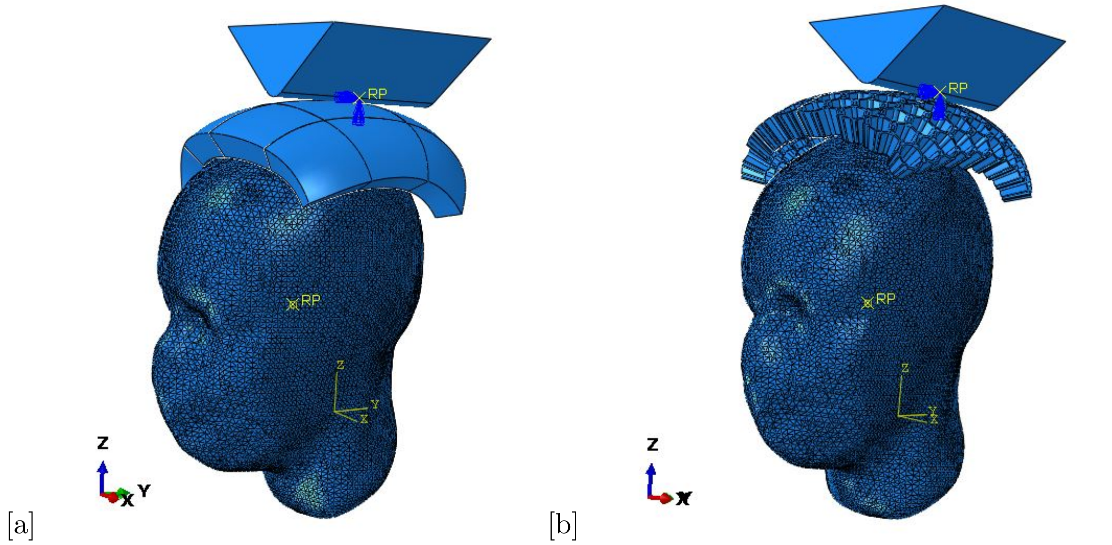

Figure 6.3: Simulation based on BS EN 1078 with head

In order to proceed with the simulation, some boundary conditions that regard ties and forces have have imposed;

- two reference points RP were created: the first in the inertia centre of the head, the second relating to the Kerbstone Anvil, which is a discrete rigid body;
- in the reference point RP of the head, in the definition of the engineering features, 5 kg was inserted for the weight and an inertia I11 = 5.64464E+07 g*mm^2, I22 = 4.60654E+07g*mm^2, I33 = 1.87302E+07g*mm^2;
- to simulate the impact it was set a speed of 4,57 m/s at the reference point RP of the head in z-axis direction;
- a general contact with normal behaviour through 'hard' contact and tangential behaviour with a coefficient of friction of 0,2;
- between the upper surface of the helmet and the impactor it has been initialized a Surface to Surface contact with normal behaviour through 'hard' contact and tangential behaviour with a coefficient of friction of 0,2; with directionality imposed on 'isotropic';
- the movement between the Kerbstone anvil and the helmet is fixed through an Encastre, therefore unable to move and rotate in x,y,z directions;
- the rotation in x, y, z relative to the RP of the rigid discrete impactor body is locked

FEM element

As reported in Table 5.3, the portion of the helmet in EPS has used a mesh with hexahedral elements of linear order. For the structure (beetle) of PLA LW, given the geometry complexity, it was necessary to use a quadratic order of tetrahedra. For the mesh of the head, instead, in both simulations have been used quadrilateral elements of linear order, as reported in the Tables 6.1 and 6.2.

Object	Element number	Elements Shape	Geometric order
Head	3755	Quadrilateral - R3D4	Linear
Head	34542	Quadrilateral - R3D3	Linear
Helmet (PLA)	272302	Tetrahedral - C3D10M	Quadratic

Table 6.1: Mesh element - Head simulation with PLA LW (beetle) helmet

Object	Element number	Elements Shape	Geometric order
Head	3755	Quadrilateral - R3D4	Linear
Head	34542	Quadrilateral - R3D3	Linear
Helmet (EPS)	72280	Hexahedral - C3D8R	Linear

Table 6.2: Mesh element - Head simulation with EPS helmet

6.2 Results

Figure 6.4 represents the simulation in line with BS EN 1078 concerning the helmet in EPS [a] and the helmet with bio-inspired structure in PLA LW. For both simulations, Van Mises' stress has Yield Stress values in the case of EPS which is 0,9 MPa, and the plastic behaviour combination of PLA LW [b].

In the case of head and Kerbstone, Anvil stress was not assessed as they were previously defined as discrete rigid bodies.

6.3 Head Injury Criterion

The HIC quantifies head impact severity by incorporating time of acceleration exposure and acceleration magnitude; it is calculated in post-processing phase with the following Equation 6.1:

$$HIC_{15} = \left[\frac{1}{(t_1 - t_2)} \int_{t_1}^{t_2} a(t)dt \right]^{2,5} (t_2 - t_1) \tag{6.1}$$

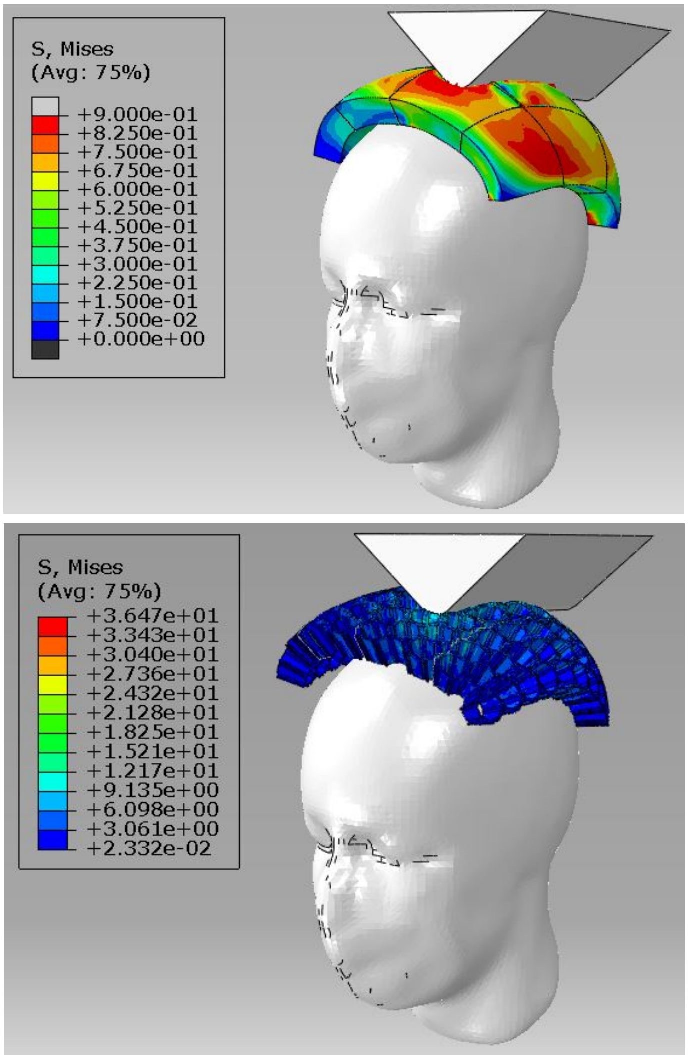

[a]

[b]

Figure 6.4: Results simulation based on BS EN 1078 with sectioned head

For this analysis, a(t) is the acceleration calculated in the centre of mass of the head (corresponding to the reference point RP) expressed in g, and the time interval $(t_2 - t_1)$ was chosen to maximize HIC over a maximum duration of 15 ms.

Matlab and the *trapz* function were used to calculate the HIC to integrate acceleration over time. t_2 and t_1 were considered initial and final times of the simulation: $t_1 = 0$ s and $t_2 = 10$ s, time less than 15 s.

HIC value of 198 was obtained for EPS and 87 for PLA LW. Considering the Hayes et al. [16] document about the HIC values and the graph in Figure 6.5 developed by the author, it is possible to find the percentages related to the different injury AIS1 - AIS6, which correspond respectively to lower and higher severity, while in Figure 6.6 the relative fatality to every value of AIS is shown. The values obtained for the HIC and other criteria are shown in Table 6.3. The HIC value for EPS is 198, for PLA LW it is

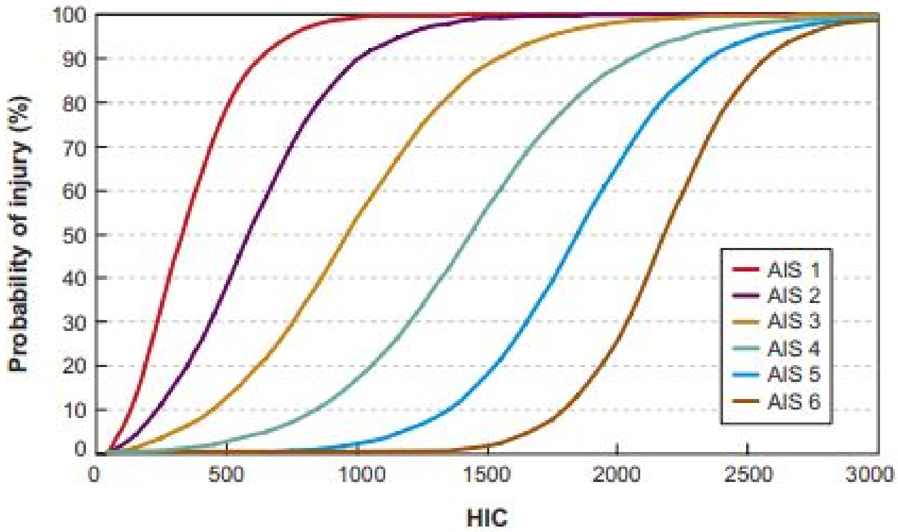

Figure 6.5: Head injury risk curves based on HIC values [16]

Injury severity AIS	Severity code	Fatality rate (range %)
1	Minor	0.0
2	Moderate	0.1–0.4
3	Serious	0.8–2.1
4	Severe	7.9–10.6
5	Critical	53.1–58.4
6	Maximum (currently untreatable)	...

Figure 6.6: The abbreviated injury score versus fatality rate [16]

87. Analyzing the data and comparing them with the curves of the Figure 6.5, I obtain:

- a percentage between 20 - 30 % of AIS 1 for EPS, 10 - 20 % for PLA LW;
- a percentage between 10 - 20 % of AIS 2 for EPS and 0 - 10 % for PLA LW;
- for AIS 3, AIS 4, AIS 5, AIS 6 the percentages for both structures is between 0 - 10 %

Comparing these percentages with the fatality rate of Figure 6.6 it is clear there is a risk of Moderate and Minor fatality in the case of EPS and PLA LW, as all values are between 0 and 30 %.

	HIC	PLA [g]	GSI	E [J]
EPS	198	97	361	37,723
PLA LW	87	75	169	44,102

Table 6.3: Head Injury Data - values

6.4 Peak Linear Acceleration

The resultant linear acceleration versus time curve was calculated according to Equation 6.2

$$\gamma(t) = \sqrt{\gamma_x^2(t) + \gamma_y^2(t) + \gamma_z^2(t)} \tag{6.2}$$

where:

- $\gamma(t)$ is the resultant linear acceleration (g),
- $\gamma_x(t)$ is the linear acceleration in x axes (g),
- $\gamma_y(t)$ is the linear acceleration in y axes (g),
- $\gamma_z(t)$is the linear acceleration in z axes (g)

The value of the impact should never exceed 250g [9]. Cripton at all. [9] in their study examined a helmet with expanded polystyrene (EPS). Figure 6.8 shows maximum HIC for helmeted and unhelmeted drops from all heights. For each drop height, helmets reduced HIC relative to unhelmeted drops. IARV value is 180g. The acceleration in the two cases is shown in Figure 6.7, and the maximum values are 97g for EPS and 75g for PLA LW as reported in Table 6.3. The two values, considering a maximum value calculated by Cripton [9] of 180g, are amply optimal and comply with the standard of 250g.

6.5 Gadd Severity Index

Gadd proposed the Severity Index Criteria shown in Equation 6.3. Following this criterion, the GSI values that are over 1000 produce serious internal head injury [33]:

$$GSI = \int_0^{t_1} a(t)^{2,5} dt \tag{6.3}$$

Where:

- a is the linear acceleration (g)
- t is the duration of the impact (s)

I calculated the GSI with the function *trapz* between 0 and t, and the resulting values are 361 for the EPS and 169 for the PLA LW, which comply with the limit.

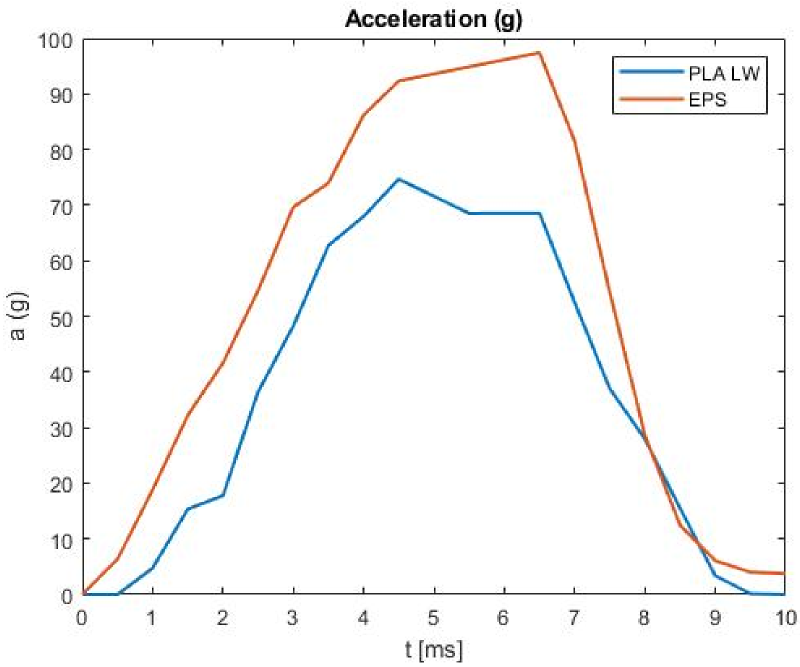

Figure 6.7: Peak accelerations for both helmets

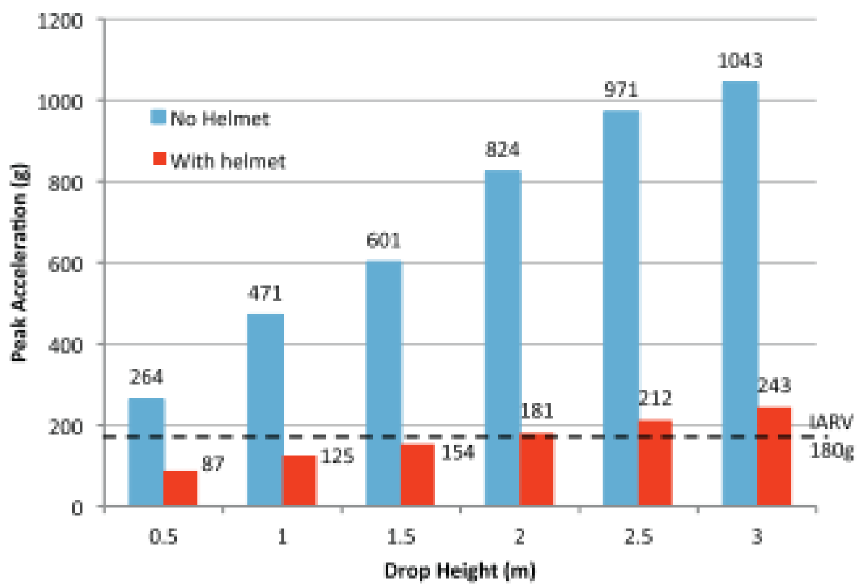

Figure 6.8: Peak accelerations for both helmeted and unhelmeted drops. Numbers over bars indicate peak acceleration; For 2 m drop height, results stated are the mean value calculated from three drops [9]

6.6 Diffuse Axonal Injury

DAI cases covered all incidences in which neurological injuries occurred as well as concussion, unconsciousness and coma.

In order to assess the risk of head trauma in terms of diffuse axonal injury (DAI), Milne et al. [23] defined a model based head injury criteria, as follows, obtaining the results in Figure 6.9:

- 50 % risk of moderate neurological injury (DAI1+): Brain Von Mises shearing stress of 28 kPa
- 50 % risk of severe neurological injury (DAI2+): Brain Von Mises shearing stress of 53 kPa

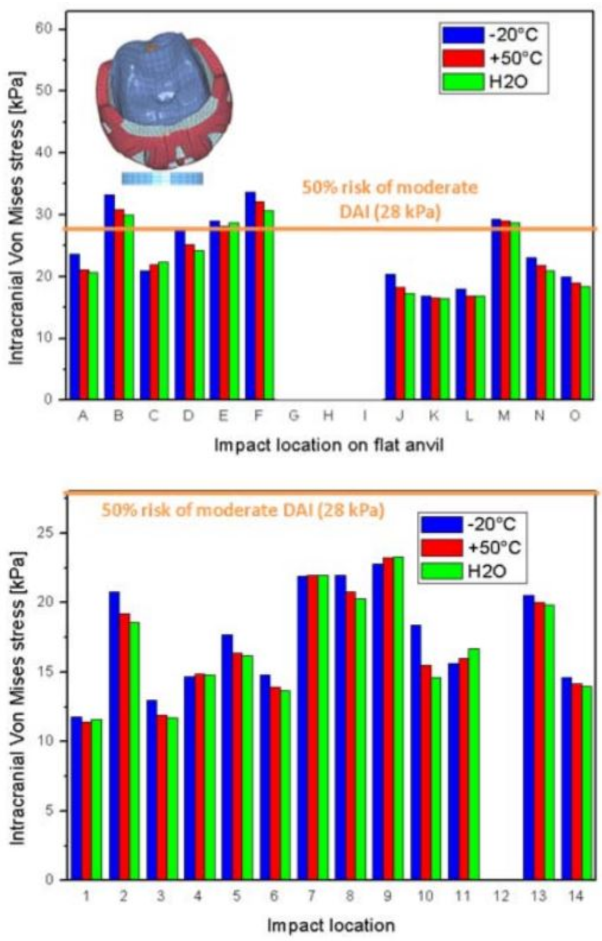

[a]

[b]

Figure 6.9: Peak intra-cerebral shearing stress computed with the helmet model coupled to the human head model for all impact points: (a) Flat anvil, (b) Kerbstone anvil [23]

6.7 Energy absorbed

In Figure 5.2, during the impact test between the kerbstone Anvil and the plan with the bio-inspired structure in PLA LW and EPS it was found that the PLA LW, although with a small difference of 10 J, absorbed more energy in comparison with the EPS. When the test is carried out in compliance with BS EN 1078 and the head with a speed of 4,57 m/s (corresponding to the kerbstone Anvil), as shown in Figure 6.10, also in this case the PLA LW with the optimized helmet structure manages to absorb more energy (even if the difference is very low) compared to the EPS. The maximum energy value in PLA LW is 44,102 J, of EPS is 37,723 J.

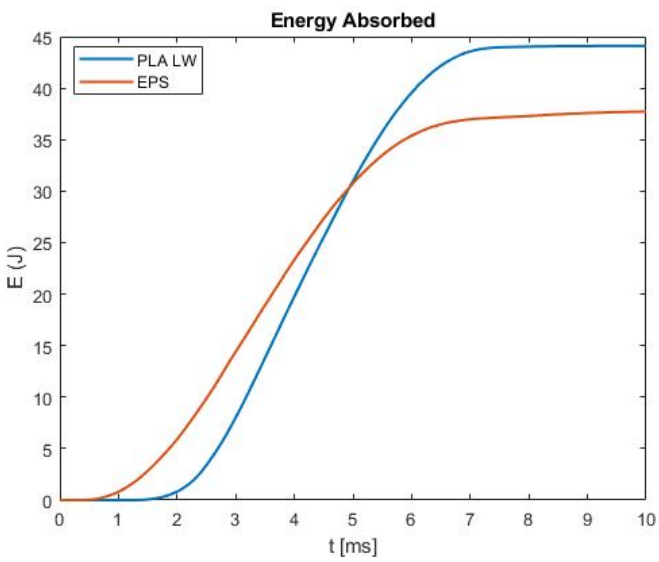

Figure 6.10: Energy absorption - BS EN 1078

Chapter 7

Conclusion

7.1 Conclusion

In this thesis work, a bicycle helmet with a bio-inspired structure in PLA LW and 3D printed was created. The initial approach was to introduce an innovative aspect to standard EPS helmets, not using foam, but a polymer, with new geometries able to absorb much energy during the impact. For this reason, the beetle structure has been preferred, relying solely on the hypothesis encountered in the literature of its quality in absorbing energy.

Combining the new material of the PLA LW and beetle structure has made possible the development of new material; satisfactory characteristics have been obtained since the first tests. The two materials were first subjected to tensile tests to determine their specific stress: in these, the PLA LW had positive results.

Subsequent dynamic physical tests were carried out on 3D printed helmet models and on reference helmets in EPS to calculate the absorption energy in both cases at the time of impact. These resulted in energy absorption of the beetle structure in PLA LW with the application of a TPU cover almost equal to that of EPS, about 50J. To validate with finite element analysis the two models, an explicit dynamic step was used in Abaqus. Simulations showed that the PLA LW structure absorbs a higher amount of energy than the EPS: the higher is 50 J and the EPS 40J.

Finally, positive results have also been obtained in calculating the head injury data, simulating according to BS EN 1078 with the use of impactor, helmet, and head. The acceleration values for both the structures were inferior to 220g, precisely for the PLA LW was 75g and for the EPS 97g. The same applies to the calculation of HIC and GSI (maximum acceptable value of 1000), where the values are 87 and 169 in the case of PLA LW and 361 and 198 in EPS. For all tests, therefore, greater efficiency of the structure in PLA LW has been obtained. Positive results also in the simulation of the energy absorbed during the impact, as the value referring to the EPS was 35J and that of the PLA LW was 45J.

7.2 Future work lines

The positive results obtained can be considered as a starting point for further tests and simulations to ensure the safety of the helmet and compliance with the regulations; but, before getting improvements and continue testing, changes are required:

- the beetle structure of the helmet made with GH adapts to the SubD without allowing to have a homogeneous distribution; it would be appropriate to have more regular hexagonal geometries;
- the mesh of the helmet is too complex and does not allow to perform the simulation; probably to use a more regular structure would have a mesh accordingly more regular, and the simulation would be successful;
- the uneven helmet structure has so many defects that the print is imperfect, and this can change the results of the impact tests: the structure should be improved;
- the printing time varies from 4 to 5 days: it should be improved;
- the TPU helmet cover is too big for the RAISE printing plan: it is necessary to generate a new geometry;
- the TPU cover it must be fixed on the helmet;
- in the calculation of the DAI it is necessary to have the definition of the brain, and the head should not be considered as a rigid body;
- in the injury calculation the helmet without protection was considered, with the TPU cover the result will be better;
- air flow analysis.

The comments mentioned are only considerations and problems that I gained during my thesis and which should be improved, but I am sure that these changes and improvements, from design to printing and simulations, can make the helmet a good product.

Bibliography

[1] K. Adanty, J. M. Clark, A. Post, Thomas Blaine H., and M. D. Gilchrist. Comparing two proposed protocols to test the oblique response of cycling helmets to fall impacts. *International Journal of Crashworthiness*, 6:648 – 663, 2020.

[2] M.F. Ashby, Y.J.M. Brechetb, D. Cebona, and L. Salvoc. Selection strategies for materials and processes. *Materials and Design*, 2004.

[3] M. Aysha. El casco de bicicleta voronoi impreso en 3d, mas seguro y ligero? https://www.3dnatives.com/en/3d-printed-bicycle-helmet-voronoi-190820204/.

[4] H. Bikas, P. Stavropoulos, and G. Chryssolouris. Additive manufacturing methods and modelling approaches: a critical review. *The International Journal of Advanced Manufacturing Technology*, 83:389–405, 2016.

[5] British Standards BSI. Helmets for pedal cyclists and for users of skateboards and roller skates - BS EN 1078. 2012.

[6] British Standards BSI. Headforms for use in the testing of protective helmets, BS EN 960. 2020.

[7] ColorFabb. Colorfabb lw-pla, 2019. "https://colorfabb.com/media/datasheets/tds/colorfabb/TDS_E_ColorFabb_LW-PLA.pdf".

[8] V. G. Coronado, T. Haileyesus, J. M. Bell T. A. Cheng, J.Haarbauer-Krupa, M. R. Lionbarger, J. Flores-Herrera, L. C. McGuire, and J. Gilchrist. Trends in sports and recreation-related traumatic brain injuries treated in us emergency departments: the national electronic injury surveillance system-all injury program (neiss-aip), 2001-2012. *J. Head Trauma Rehabil.*, 30:185–197, 2015.

[9] P. A Cripton, D. M. Dressler, D. Stuart, Cameron A, Christopher R, and D. Richards. Bicycle helmets are highly effective at preventing head injury during head impact: Head-form accelerations and injury criteria for helmeted and unhelmeted impacts. *Accident Analysis and Prevention*, 70:1–7, 2014.

[10] L. Cui, M. A Forero R., and M. D. Gilchrist. Optimisation of energy absorbing liner for equestrian helmets. *UCD School of Electrical, Electronic and Mechanical Engineering, University College Dublin, Belfield, Dublin4, Ireland*, 2020.

[11] C. Deck, N. Bourdet, F. Meyer, and R. Willinger. Protection performance of bicycle helmets. *Journal of safety research*, pages 67–77, 2019.

[12] Committee F08. Specification for headforms, F2220. *ASTM International*, 2015.

[13] Committee F08. Specification for helmets used in recreational bicycling or roller skating, F1447. *ASTM International*, 2018.

[14] Committee F08. Test methods for equipment and procedures used in evaluating the performance, F1446. *ASTM International*, 2020.

[15] P. Halldin. Shock absorption including measuring. *CEN/TC 158 Working Group 11*, 2018.

[16] W. C. Hayes, M. S. Erickson, and E. D. Power. Forensic injury biomechanics. *Annual review of biomedical engineering*, pages 55–86, 2007.

[17] HEXR. "https://hexr.com/".

[18] C. Jinxiang, Z. Xiaoming, O. Yoji, S. Kazuya, G. Zhensheng, and P. Longcheng. The deformation mode and strengthening mechanism of compression in the beetle elytron plate. *Materials and Design*, 131:481–186, 2017.

[19] S. Kroeker, M. Ozkul, A. De Marco, S. Bonin, and G.P. Siegmund. Density variation in the expanded polystyrene eps foam of bicycle helmets and its influence on impact performance. *Journal of biomechanical engineering*, 2019.

[20] S. G. Kroeker, S.J. Bonin, A. L. DeMarco, C. A. Good, and G. P. Siegmund. Age does not affect the material properties of expanded polystyrene liners in field-used bicycle helmets. *Journal of biomechanical engineering*, 2016.

[21] M. Meier, K. H. Tan, M. K. Lim, and L. Chung. Unlocking innovation in the sport industry through additive manufacturing. *Business Process Management Journa*, 2018.

[22] N. J. Mills and A. Gilchrist. The effectiveness of foams in bicycle and motorcycle helmets. *Accident Analysis Prevention*, 23:153 – 163, 1991.

[23] G. Milne, C. Deck, R. P. Carreira, Q. Allinne, and R. Willinger. Development and validation of a bicycle helmet: assessment of head injury risk under standard impact conditions. *Computer methods in biomechanics and biomedical engineering*, 15 Suppl 1:309 – 310, 2012.

[24] Y. Mosleh, S. J. Vander, B. Depreitere, and J. Ivens. Novel composite foam concept for head protection in oblique impacts. *Adv. Eng. Mater. (Advanced Engineering Materials)*, 10, 2017.

[25] H. Mustafa, T. Y. Pang, T. Ellena, and S. H. Nasir. Impact attenuation of user-centred bicycle helmet design with different foam densities. *J. Phys.: Conf. Ser. (Journal of Physics: Conference Series)*, 1150, 2019.

[26] S. H. Ngoc and L. Guoxing. A review of recent research on bio-inspired structures and materials for energy absorption applications. *Composites Part*, 181, 2020.

[27] J. I. Novak and A. R. Novak. Is additive manufacturing improving performance in sports? a systematic review. *Sport engineering and technology*, 13, 2020.

[28] European Road Safety Observatory. European road safety observatory facts and figures - cyclists - 2020, December 2020. "https://ec.europa.eu/transport/road_safety/sites/default/files/facts_figures_cyclists_final_20210323.pdf".

[29] New York City Departments of Health, Parks Mental Hygiene, Transportation Recreation, and the New York City Police Department. Bicyclist fatalities and serious injuries in new york city. 2005.

[30] W. Pengwen, Y. Jing, H. Yanan, H. Jiaofei, and F. Xiaoyang. Innovative design of a helmet based on reverse engineering and 3d printing. *Alexandria Engineering Journal*, 60:3445–3453, 2021.

[31] S. G. Piland, T. E. Gould, M. Jesunathadas, J. S. Wiggins, O. McNair, and V. C. Shane. Protective helmets in sports. *Materials in Sports Equipment*, 3, 2019.

[32] K. Schmitt, P. F. Niederer, M. H. Muser, and F. Walz. Trauma biomechanics. *Springer Berlin Heidelberg*, 2010.

[33] David Sepélveda López. *A Biomechanical Analysis of Bicycle Helmets using FEM*. PhD thesis, 2019. Bachelor thesis.

[34] H. Stigson. *Bicycle Helmets 2020 Tested by Folksam*. PhD thesis, 2020. PhD Associate Professor Traffic Safety Research.

[35] H. Tao, K. Sudip, N. Anindya, and X. Yongzhao. 3d printed sensors for biomedical applications: A review. *sensor*, 2019.

[36] M. Trzaskalska and R. Chwastek. Damping properties and density of helmet liners made of expanded polystyrene (eps). *Archives of Metallurgy and Materials*, 66, 2020.

[37] Crupi V., Epasto G., and Guglielmino E. Impact response of aluminum foam sandwiches for light-weight ship structures. *Metals*, 1:98–112, 2020.

[38] W. Wei-cai, F. Dong-ming, and L. Yuan-xin. Study on impact energy absorbing performance of eps buffer layer of motorcycle helmet. *Proceedings - 2013 International Conference on Mechanical and Automation Engineering, MAEE*, 2013.

[39] Z. Xiaoming, C. Jinxiang, O. Yoji, Z. Peiwei, X. Xiaobing, and Y. Xindi. Influence of honeycomb dimensions and forming methods on the compressive properties of beetle elytron plates. *Journal of Sandwich Structures and Materials*, 22:28–39, 2020.

[40] S. Zhi, L. Dong, Z. Weisheng, S. Shanshan, and G. Xu. Topological optimization of biomimetic sandwich structures with hybrid core and cfrp face sheets. *Composites Science and Technology*, 142:79–90, 2017.

[41] S. Zhi, S. Shanshan, G. Xu, H. Xiaozhi, and C. Haoran. On compressive properties of composite sandwich structures with grid reinforced honeycomb core. *Composites Part B*, 94:245–252, 2016.